Journal of Hydrology 612 (2022) 128242

Contents lists available at ScienceDirect

Journal of Hydrology

journal homepage: www.elsevier.com/locate/jhydrol

Research papers

Linking fire-induced evapotranspiration shifts to streamflow magnitude and timing in the western United States

Natalie M. Collar [a,b,*,1], Samuel Saxe [c,2], Brian A. Ebel [d,3], Kathryn S. Boden [a,4], Ashley J. Rust [a,5], Terri S. Hogue [a,6]

[a] Colorado School of Mines, Department of Civil and Environmental Engineering, 1500 Illinois St., Golden, CO 90336, USA
[b] Wright Water Engineers, Inc., 2460 W 26th Ave. Ste 100A, Denver, CO 80211, USA
[c] U.S. Geological Survey, Analysis and Prediction Branch, Lakewood, CO 80225, USA
[d] U.S. Geological Survey, Water Resources Mission Area, Shelburne, VT 05482, USA

ARTICLE INFO

This manuscript was handled by Nandita Basu, Editor-in-Chief, with the assistance of Xue Feng, Associate Editor

Keywords:
Remote sensing
SSEBop
S-ARIMA
Lagged regression
Disturbance hydrology
ET
Wildfire

ABSTRACT

The impact of wildfire on water availability is a critical issue in the western United States. Because actual evapotranspiration (ETa) constitutes the largest loss in the terrestrial water budget, it has been suggested that fire-induced ETa reduction is a primary driver of elevated post-fire discharge. Ten gaged watersheds with burns exceeding 5% of their total contributing drainage area were selected from California, Oregon, Montana, Utah, New Mexico, and Colorado. Continuous daily stream gage data were compiled, and 30-meter ETa estimates were calculated with the Operational Simplified Surface Energy Balance (SSEBop) model. Fire-induced ETa shifts were quantified with statistical tests that compared pre and post-fire monthly ETa in burned and unburned pixels; the dampening effect of scale was also evaluated by repeating tests on all pixels from the entire basin. As streamflow data are point measurements that aggregate a large spatial area, additional statistical methods were required to isolate the effect of fire from climate on baseflow and runoff. Key findings include a) significant fire-induced ETa reductions were only distinguishable in basin-scale monthly datasets when at least 73% of the basin burned, b) the effect of wildfire disturbance on streamflow magnitude was seasonably variable, c) streamflow was modified in basins with as little as 6% burned drainage area; however, shifts only persisted beyond the fifth post-fire year where more than three-quarters of the basin was fire-impacted, and d) surplus water from ETa reduction was sufficient to account for boosted fire-induced streamflow. Where fire-induced streamflow increases were not significantly correlated with ETa anomaly, other fire-impacted landscape processes may have contributed to modified runoff generation and routing. Where fire reduced ETa but streamflow shifts were not detected, compensatory ETa pathways may have consumed the excess water before it reached the gage. Findings suggest

Abbreviations: ACF, autocorrelation function; ADF, augmented Dickey-Fuller test; AIC, Akaike Information Criteria; bf, baseflow; BIC, Bayesian Information Criteria; CI, confidence interval; EPA, United States Environmental Protection Agency; ETa, actual evapotranspiration; ETo, reference evapotranspiration; ETp or PET, potential evapotranspiration; ET/P, evaporation ratio; GEE, Google Earth Engine; gNATSGO, Gridded National Soil Survey Geographic Database; IQR, inter-quartile range; LM, linear model; LST, land surface temperature1; MLE, maximum likelihood estimation; MTBS, Monitoring Trends in Burn Severity; NCAR, National Center for Atmospheric Research; NDVI, Normalized Difference Vegetation Index; NHD, National Hydrography Dataset; NLCD, National Land Cover Database; NRCS, USDA Natural Resources Conservation Service; PACF, partial autocorrelation function; Ppt, precipitation; PRISM, Parameter-elevation Regressions on Independent Slopes Model; ro, runoff; S-ARIMA, seasonal autoregressive integrated moving average model; SPI, Standardized Precipitation Index; SSEBop, operational Simplified Surface Energy Balance Model; TOA, top-of-atmosphere; Ts, land surface temperature; USDA, United States Department of Agriculture; USGS, United States Geological Survey; WSS, NRCS's web soil survey.

* Corresponding author at: Colorado School of Mines, Department of Civil and Environmental Engineering, 1500 Illinois St., Golden, CO 90336, USA.
E-mail addresses: ncollar@wrightwater.com (N.M. Collar), ssaxe@usgs.gov (S. Saxe), bebel@usgs.gov (B.A. Ebel), kboden@mines.edu (K.S. Boden), arust@mines.edu (A.J. Rust), thogue@mines.edu (T.S. Hogue).
[1] ORCID-ID: 0000-0003-4711-0090.
[2] ORCID-ID: 0000-0003-1151-8908.
[3] ORCID-ID: 0000-0002-5413-3963.
[4] ORCID-ID: 0000-0002-0588-7662.
[5] ORCID-ID: 0000-0002-9759-8285.
[6] ORCID-ID: 0000-0003-1524-8896.

https://doi.org/10.1016/j.jhydrol.2022.128242
Received 7 March 2022; Received in revised form 13 July 2022; Accepted 17 July 2022
Available online 22 July 2022

that water providers with small source-water collection areas have higher relative risk for fire-induced hydromodification than providers with larger or more diversified supply portfolios. Results also illustrate the tendency of overarching climate signals to mask or artificially boost the apparent effect of landscape disturbance on streamflow at the basin outlet.

1. Introduction

Severe and erratic wildfire behavior has become more common since at least the mid-1980 s and is causing concern in the western United States (Bladon et al., 2014; Chow et al., 2021; Hallema et al., 2018; Martin, 2016; Murphy et al., 2018). Substantial effort is being spent to identify short and long-term fire wildfire trends (Crawford et al., 2015; Parks and Abatzoglou, 2020), fire's role in landscape ecology (David et al., 2018; Lake et al., 2017) and geomorphology (Keller et al., 2019; Shakesby and Doerr, 2006), and the risks posed by wildfire to built and natural environments (Martin et al., 2016). Despite progress in identifying and understanding critical processes, the location-specific effects of wildfire-related forest disturbance on downstream water supplies remain unclear. Additional uncertainty is introduced by the confounding pressures of climate aridification (Overpeck and Udall, 2020) and increasing climate variability (van der Wiel and Bintanja, 2021; Zhuang et al., 2021) as they often co-occur with wildfire activity in forested watersheds.

Reports of increased flooding, hillslope erosion, debris flows, landslides, reservoir sedimentation, and water quality degradation following wildfire are common in the American West and elsewhere (Burke et al., 2013; Emelko et al., 2016; Moody and Martin, 2009; Nunes et al., 2018; Nyman et al., 2020; Rust et al., 2018; Santi and Morandi, 2013; Saxe et al., 2018). Concurrently, the mechanistic linkage between actual evapotranspiration (ETa) and streamflow has been demonstrated (Goeking and Tarboton, 2020; Goulden and Bales, 2014; Kirchner et al., 2020; Kirchner and Allen, 2020), suggesting a physical connection between ETa and the aforementioned fire-exacerbated hydrogeomorphic hazards. Such a linkage would be sensible as a) ETa is the most sensitive hydrologic component to vegetation changes, and b) it is often the largest loss in terrestrial water budgets, making it a principal arbiter of precipitation partitioning (Neary et al., 2005). However, the direction and magnitude of post-fire ETa and streamflow shifts are often variable, especially where topographic, climatic, and ecologic gradients are steep (Blount et al., 2020; Collar et al., 2021; Goeking and Tarboton, 2020; Kinoshita and Hogue, 2015; Ma et al., 2020; Saxe et al., 2018).

ETa is a spatially and temporally varying process because the systems that control it are themselves fluctuating over space and time. At a single location, the ETa rate may be a function of surface energy fluxes and states (e.g., net radiation, sensible and latent heat exchange, reflective properties of a body), surface meteorology (e.g., precipitation, wind speed, relative humidity, surface aerodynamic skin temperature), biophysical controls (e.g., soil moisture-holding capacity, stomatal conductance, rooting structure, aerodynamic resistance of the plant canopy), and landscape characteristics (e.g., topography, additional sources of roughness) (Chang, 2012; Lettenmaier et al., 2015; Maidment, 1993; Neary et al., 2005). The timescales at which the states or rates of ETa's drivers range are considerable: precipitation, for example, has variable intensity during a single storm event as well as in accordance with multi-year cycles (e.g., decadal oscillations), longer-term trends (e.g., anthropogenic climate change), and hydroclimatic processes (e.g., glaciation) (Beyene et al., 2021; Eskridge et al., 1997; Xu et al., 2014). Even at the same location, the ETa flux can be energy or water-limited depending on seasons and over interannual timescales (Budyko, 1974; Ryu et al., 2008; Xu et al., 2014). As an added layer of complexity, many of the variables that control ETa rates are vulnerable to abrupt modification from acute landscape disturbance (Jin et al., 2012; Sexstone et al., 2018; Slinski et al., 2016).

Downstream, quantifying the effect of landscape disturbance on streamflow is challenging as prevailing climate (precipitation, air temperature, potential evapotranspiration (ETp or PET)) can drive a majority of observed streamflow variability in undeveloped watersheds (Bart et al., 2016; Bart and Tague, 2017; Jaramillo and Destouni, 2014). This is especially the case where the percentage of disturbed contributing drainage area is relatively small because the explanatory power of the overarching climate signal can easily mask or exaggerate the apparent effects of the disturbance at the gage (Hallema et al., 2018). Readily available remotely sensed data and reanalysis products bring this challenge to the forefront because they enable before-after/control-impact evaluations to be conducted via observation of the same location through time where a paired (reference) watershed approach may have been used otherwise (Conner et al., 2016; Downes et al., 2002; Eberhardt, 1976). The need to identify and monitor a reference basin is removed as pre-fire observations from the disturbed area can be used as a control, however, climate signals can no longer be accounted for by comparing the disturbed and reference basins (Beyene et al., 2021; Goulden and Bales, 2014; Hallema et al., 2017). Numerous studies have proposed statistical and process-based methods for separating the effects of landscape drivers from climate drivers on catchment runoff and baseflow (Bart and Tague, 2017; Beyene et al., 2021; Cong et al., 2009; Hallema et al., 2018; Kurzweil et al., 2021; Wine et al., 2018; Xu et al., 2014), thus providing an analytical framework for quantifying linked fire effects on ETa and streamflow. Most have reported results at the annual timestep.

Natural resource managers need to understand the scale(s) at which fire-induced hydrologic shifts become meaningful for source-water hydrology. The current study seeks to address that need by evaluating statistical linkages between fire-induced ETa modification and streamflow at varying spatiotemporal scales. We examine two primary research questions: a) How does wildfire modify monthly ETa, baseflow, and runoff at basins in the western United States? And b) To what degree are fire-induced streamflow shifts explained by the ETa shifts? Previously proposed procedures for separating the effects of landscape from climate drivers are implemented for annual time series evaluation and improved upon for sub-annual time series evaluation.

2. Methods

2.1. Overview

Monthly 30-meter (m) ETa data were calculated at ten burned basins in the western United States with the Operational Simplified Surface Energy Balance (SSEBop) model (Senay, 2018; Senay et al., 2013). Daily streamflow data and static basin attributes were acquired at basin-scale resolution; additional meteorologic and landscape variables were extracted at 30-m pixel-scale resolution. Fire-induced ETa shifts were quantified with statistical tests that compared pre and post-fire monthly and yearly ETa in burned and unburned pixels; timing of significant ETa shifts were also identified with change point detection tests and compared to fire event dates. Because pixel-scale data were not available for streamflow, additional statistical methods were used to disentangle the effect of fire from climate on post-fire baseflow and runoff at both monthly and annual time steps. Relationships between fire-induced streamflow shifts, ETa and precipitation anomalies, annual water demand, and basin characteristics were explored. A conceptual overview of the study's input data, data processing steps, statistical tests applied, statistical models constructed, and results is provided in Fig. 1.

2.2. Basin selection

Study basins were selected using the following criteria: a) the basin was in the western United States (west of the 100th meridian); b) more than 5 % of the basin was burned by a wildfire in a single water year (October 1 through September 30) according to the Monitoring Trends in Burn Severity (MTBS) dataset (Eidenshink et al., 2007); c) no additional burns comprising more than 2 % of the basin's total drainage area occurred in the ten years before or after the water year of interest; d) daily United States Geological Survey (USGS) stream gage data were available at the basin outlet for the entire study period (one exception made); and e) the basin did not contain manmade hydraulic control structures capable of modifying the timing, rate, and/or volume of streamflow at the gage.

Only eleven basins were identified in the western United States that met all five study criteria. Ten of them were included in the current study (Figs. 2A and 2B, Table 1) while southern California's Devil Canyon was excluded due to its inclusion in a similar study (Kinoshita and Hogue, 2015). The other basin studied in Kinoshita and Hogue, 2015, City Creek, was excluded from the current study because the majority of it burned twice in six years (2003 Old Fire, 1997 Hemlock Fire). The authors acknowledge that the relatively small number of study basins included in the current study limits the reach and applicability of our results to the entire western United States in general.

Watershed boundaries were delineated in Streamstats (https://www.usgs.gov/mission-areas/water-resources/science/streamstats-streamflow-statistics-and-spatial-analysis-tools). Burn perimeters were obtained from MTBS and clipped to basin extents where necessary. The percentage of burned contributing drainage area was calculated in ArcPro (version 2.9) and ranged from 6 to 88 %. In all but one watershed, only one burn event (defined by MTBS event ID) was responsible for the total burned area in the basin during the water year of interest. The exception occurred in Oregon's South Umpqua River basin during water year 2002, where five MTBS-mapped fires occurred to comprise 23 % of the basin's total drainage area.

2.3. Data collection

2.3.1. Ssebop evapotranspiration

Monthly 30-m ETa was calculated at each basin for the 21-year study periods with the SSEBop model (5,284,834 pixels total). Inputs of Normalized Difference Vegetation Indices (NDVI), cloud masks, and land surface temperature (Ts) were retrieved from Landsat 7 and 8 Collection 1 Tier 1 calibrated top-of-atmosphere (TOA) reflectance data in the Google Earth Engine (GEE) Data Catalog (https://developers.google.com/earth-engine/datasets/). Auxiliary data used in the model include GridMET reference ET (ETo) (Abatzoglou, 2013) and Daymet air temperature (Thornton et al., 2018). ETa was calculated by applying a thermal index approach to combine ETp with Ts ET fractions using predefined, seasonally dynamic boundary conditions unique to each pixel

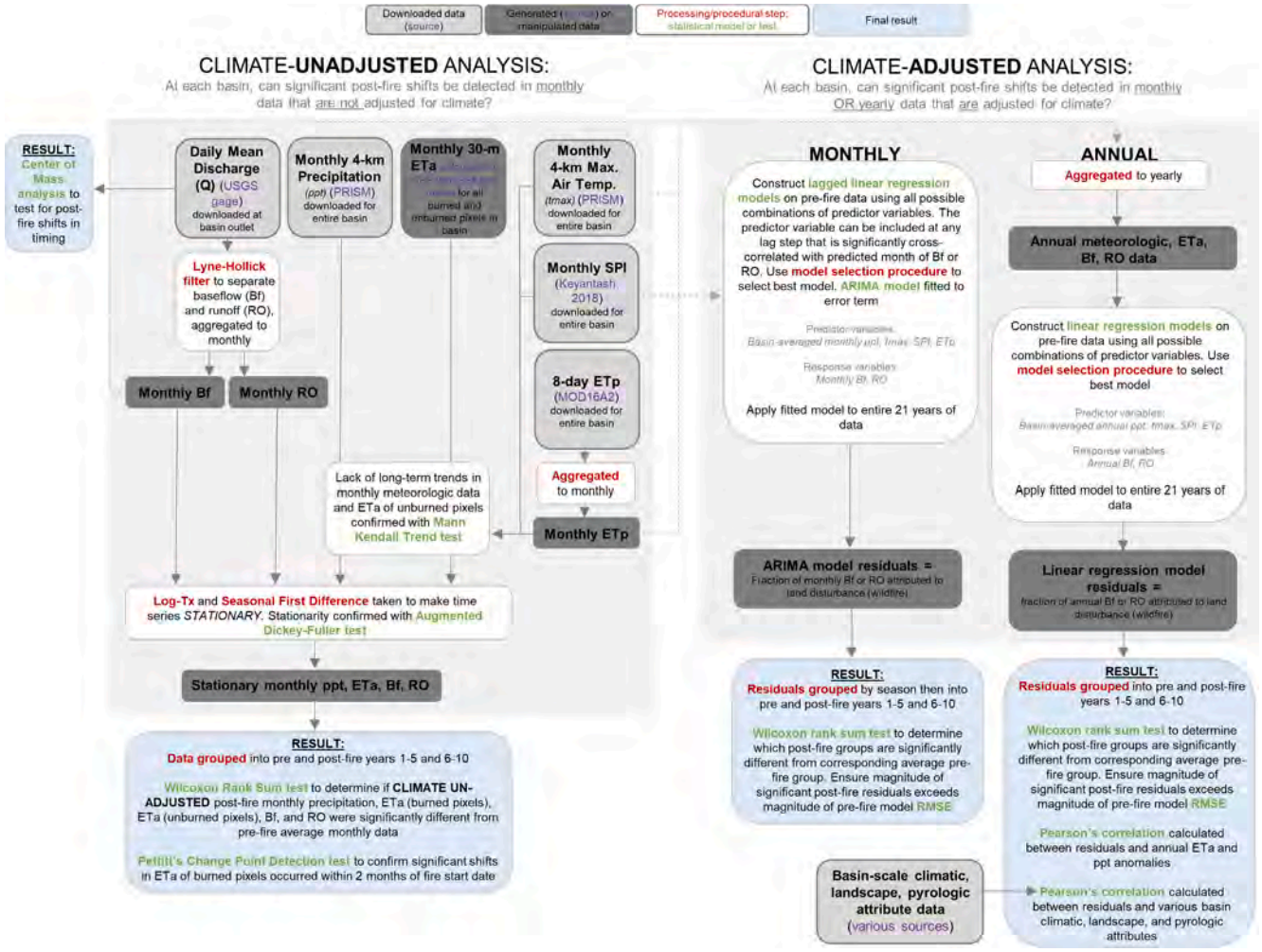

Fig. 1. Conceptual overview (flow chart) of general study methods. Items include the datasets downloaded (light grey boxes) and generated (dark grey boxes), data source information (purple font), processing/procedural steps undertaken (red font), statistical models constructed and statistical tests applied (green font), and the final study results (light blue boxes). (For interpretation of the references to colour in this figure legend, the reader is referred to the web version of this article.)

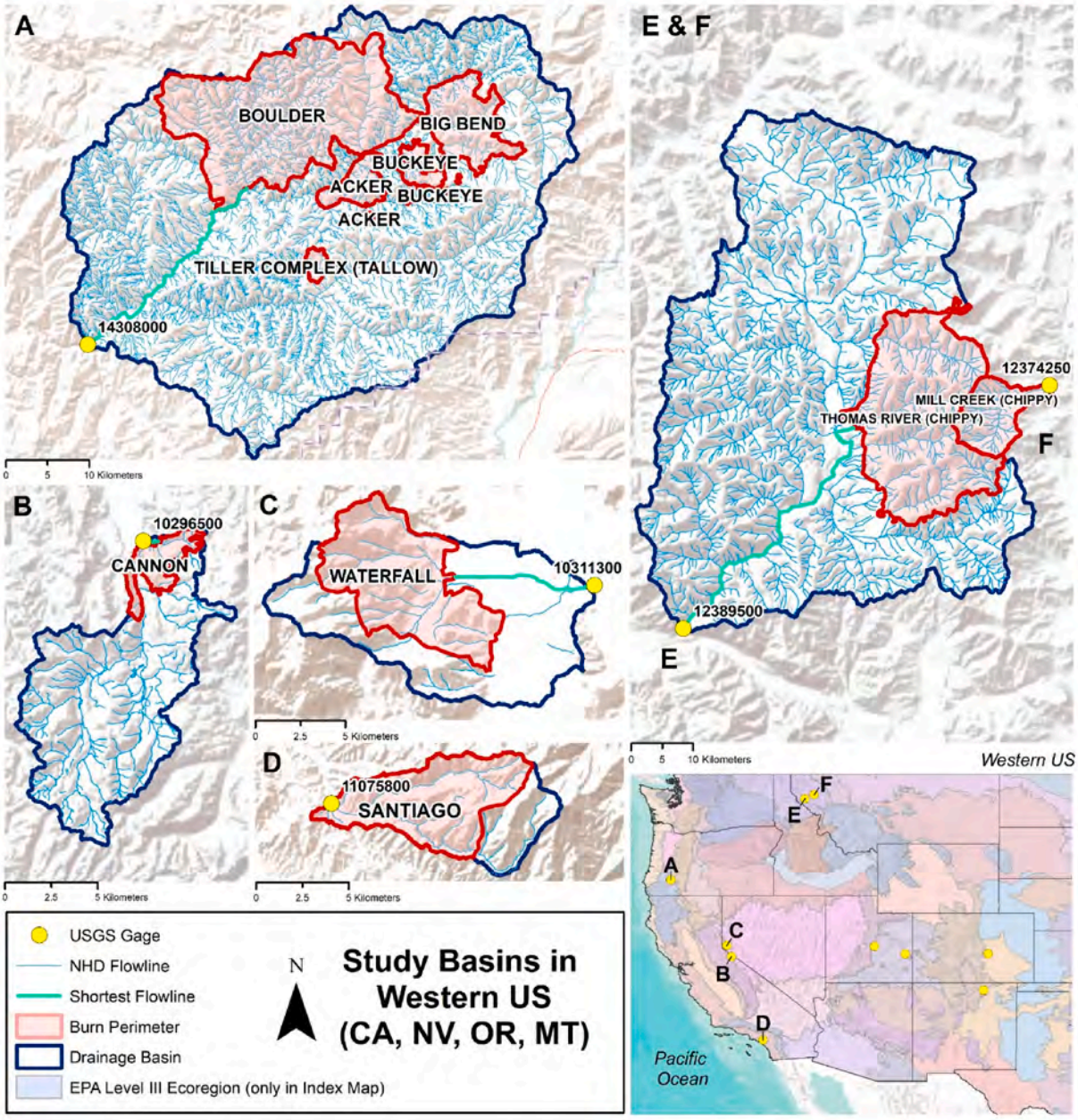

Fig. 2A. Location map of burned basins in western United States showing EPA Level III Ecoregions in index map (Omernik and Griffith, 2014). Bolded name is name of the fire event. NHD is the National Hydrologic Dataset showing flowlines.

for 'cold/wet' and hot/dry' reference points (Bastiaanssen et al., 1998; Senay, 2018).

The SSEBop model was implemented using the 'openet-ssebop' Python module (github.com/openet) developed as part of the OpenET project (https://openetdata.org/). Data were processed on the GEE platform through the Python 'ee' client library (github.com/google/earthengine-api). Our final ETa datasets are available on USGS ScienceBase (https://www.sciencebase.gov/catalog/item/628e58f9d34ef70cdba3feda).

We note that fine resolution (10 to 100-m) Landsat-based SSEBop ETa estimates have been generated for multiple studies (Dias Lopes et al., 2019; Senay et al., 2016; Sharma and Tare, 2018; Singh and Senay, 2015). Comparison of Landsat-based ETa estimates with eddy covariance flux towers and water balance data have generally shown good agreement (R^2 from 0.74 to 0.95 and Nash-Sutcliffe model efficiency (NSE) from 0.66 to 0.91) (Senay et al., 2016). Comparisons with ETa calculated by the Bowen ratio method had an R^2 of 0.82 and root mean square error (RMSE) of 0.89 mm/day (Dias Lopes et al., 2019).

2.3.2. *Streamflow*

Daily streamflow data were obtained for each basin from the USGS National Water Information System (U.S. Geological Survey, 2021) for each 21-year study period (Table 1) with one exception (only eight years of post-fire data were available for Utah's Porcupine Fire basin (https://waterdata.usgs.gov/nwis/uv/?site_no=09182400)). The Lyne-Hollick digital recursive filter was applied to separate baseflow from daily mean streamflow with the *hydrostats* R package and the alpha filtering parameter set to the default 0.975 value (Bond, 2021; Ladson et al., 2013). Runoff was calculated as the residual of the native daily mean flow rate and the calculated mean daily baseflow rate generated in the previous step. The daily baseflow and runoff time series were converted from flow rates (feet^3/second, cfs) to depths (millimeters, mm)

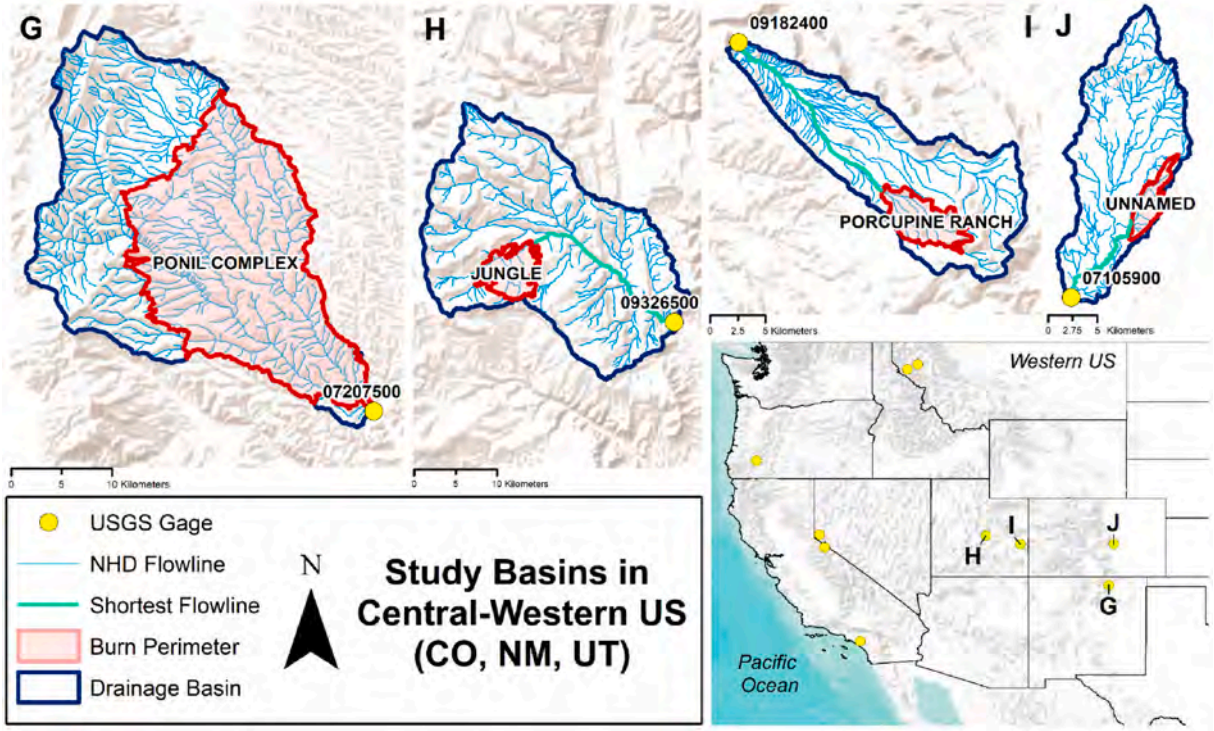

Fig. 2B. Location map of burned basins in central-western United States. Bolded name is name of the fire event. NHD is the National Hydrologic Dataset showing flowlines.

using the drainage area of each basin and aggregated to monthly and yearly totals.

2.3.3. *Additional meteorologic and landscape variables*

Additional pixel-scale meteorologic and landscape variables were extracted at each study basin including pyrologic data (e.g., fire origin data, burn severity class), pre-fire vegetation type, topographic variables (elevation, slope), and pre-fire beetle infestation. Static and dynamic basin-scale data were compiled including the length of the shortest flow path between the burn scar and stream gage, average basin soil erodibility and rainfall erosivity, the average percent of precipitation that falls as snow, average depth to a restrictive subsurface layer, and monthly Standardized Precipitation Index (SPIs) rank. Full details of datasets and extraction and aggregation procedures are provided in SI Appendix A.

2.4. *Statistical analysis*

2.4.1. *Quantifying the effect of fire on ETa and streamflow*

Since pixel-scale ETa flux was estimable from remotely sensed observations, the effect of fire could be distinguished from climate in the ETa data by running separate statistical tests on burned and unburned pixels from the same basin and comparing results. For basins that experienced burns in only a portion of their drainage area, the dampening effect of scale (in terms of both overall basin size and the muting effect of unburned contributing drainage area on basin-scale data summaries) was also evaluated by repeating the same statistical tests on all pixels from the entire basin.

Conversely, stream gage data were only available at main basin outlets as there were no nested monitoring stations in upgradient subbasins. Thus the comparison procedures used to parse the effects of fire from climate and scale in ETa data were not applicable. To avoid the need for comparative analyses of streamflow data from nearby control (unburned) basins, two additional analyses were conducted on the streamflow time series that involved the removal of the climate signal from the streamflow record altogether (Fig. 1).

2.4.1.1. Eta. At each basin, monthly ETa data were separated into groups of burned pixels, unburned pixels, and all pixels in the entire basin, and the monthly average of each group was calculated. Mann Kendall tests were applied with the *Kendall* R package (McLeod, 2011) to test for the presence of underlying trends in the ETa of the unburned pixels and in the climate variables. Following, attempts were made to make the data stationary (i.e., mean, variance, and autocorrelation structure are time invariant (Hyndman and Athanasopoulos, 2018; Milly et al., 2008; Shumway and Stoffer, 2016)). Data were log-transformed to stabilize fluctuations in variance and a seasonal first difference was taken to remove seasonal patterns (i.e., 'deseason' the data) (annual and monthly fluxes provided in SI Figure A and SI Figure B, example of deseasoning procedure provided in SI Figure C). To determine if outputs from the deseasoning procedure were seasonally stationary, autocorrelation plots (ACFs) were visually inspected and Augmented Dickey-Fuller tests (ADF) were applied with the base CRAN *tseries* R package (Trapletti et al., 2021). The ADF is a unit root test, where a unit root is a non-stationary feature of a stochastic process that can interfere with the ability to make statistical inferences from a time series model. Inability to reject the null hypothesis ($p > \alpha$, $\alpha = 0.05$) indicated the series remained seasonally non-stationary (presence of a unit root) (Shumway and Stoffer, 2016).

The deseasoned ETa data were indexed by period (ten-year pre-fire period, post-fire years one through five, and post-fire years six through ten). Non-parametric Wilcoxon rank sum tests were run on each of the ETa groups (burned pixels, unburned pixels, all pixels) to identify statistically significant shifts in either of the post-fire periods relative to the pre-fire period ($\alpha = 0.05$). Non-parametric Pettitt's change point detection tests were also applied to each time series with the *trend* R package (Pohlert, 2020) to independently check the timing of major behavioral shifts; dates of significant shifts ($\alpha = 0.05$) were compared to fire event dates. Pettitt's, based on Mann-Whitney-two-sample rank-based tests, detects a single change at an unknown point in time. It is

Table 1

Select basin and fire attributes. Total number of pixels (burned + unburned) included in analysis: 5,455,350. Total number of burned pixels included in analysis: 1,232,142. Drainage area obtained from USGS gaging station information (https://waterdata.usgs.gov) and cross-checked in ArcPro; ArcPro calculation governed. The shortest distance from the burn perimeter to the basin outlet (gaging station) was calculated using the National Hydrography Dataset in ArcPro. Percent of annual precipitation that falls as snow was obtained as a single value for each basin from the GAGESII dataset (https://water.usgs.gov/GIS/metadata/usgswrd/XML/gagesII_Sept2011.xml). Depth to any restrictive layer obtained from the NRCS WSS. Pyrologic information obtained from the MTBS database. Elevation ranges from Landfire dataset. Pre-fire dominant vegetation type ('Pre-fire dom.veg.' right-most column) is the mode of NLCD land cover class for the NLCD raster most recently preceding the fire origin date each fire at each timestep (available for years 2001, 2004, 2006, 2008, 2011, 2013, 2016). No raster was available for the Unnamed fire before the burn event (fire occurred in 1996) however, a review of Google Earth aerial imagery suggests pre-fire vegetation type was grassland/herbaceous. Detailed information on data sources and extraction and processing procedures provided in SI Appendix A.

Basin Name (State)	USGS Gage ID	Drainage Area (km^2)	Drainage Area Burned (%)	Shortest Distance from Burn Perimeter to Gage (km)	Annual Precip. that Falls as Snow (%)	Depth to Any Restrictive Layer (cm)	Fire Name	MTBS ID	Incident Type	Ignition Date	Burned Area at Mod. and High Severity (%)	Elevation Range (m)	Pre-fire dom. veg.
South Umpqua River (OR)	14308000	1167	23	36	20	>200	Boulder	OR4311312273420020713	Wildfire	7/13/2002	31	408-1691	
							Buckeye	OR4305712257520020713	Wildfire	7/13/2002	20	771-1584	
							Big Bend	OR4311061225392020714	Wildfire	7/14/2002	17	809-1742	
							Tiller Complex	OR4299412270220020715	Wildfire	7/15/2002	10	804-937	
							Acker	OR4304412264920020715	Wildfire	7/15/2002	18	484-1249	
W Walker River (CA)	10296500	632	8	3	72	101	Cannon	CA3848811946420020615	Wildfire	6/15/2002	77	1680-2675	
Mill Creek (MT)	12374250	51	88	0	43	>200	Chippy *(Mill)*	MT4780711483420070731	Wildfire	7/31/2007	66	921-2149	
Thomas River (MT)	12389500	1652	15	58	51	>200	Chippy *(Thomas)*	MT4780711483420070731	Wildfire	7/31/2007	72	988-2271	
Ferron Creek (UT)	9326500	359	6	25	47	188	Jungle	UT3914711139320070628	Wildfire	6/28/2007	31	2385-3263	
Ponil Creek (NM)	7207500	480	53	0	20	150	Ponil Complex	NM3668210504720020608	Wildfire	6/8/2002	53	2029-2842	
Castle Creek (UT)	9182400	138	11	23	52	189	Porcupine Ranch	UT3856110929920080827	Wildfire	8/27/2008	67	1859-3257	
Santiago Creek (CA)	11075800	35	73	0	0	50	Santiago	CA3372011766020071021	Wildfire	10/21/2007	72	369-1393	
Jimmy Camp Creek (CO)	7105900	170	6	16	7	148	Unnamed	CO3876010460719960224	Wildfire	2/24/1996	66	1743-1869	
Eagle Valley Creek (NV)	10311300	75	41	8	38	95	Waterfall	NV3917011981620040714	Wildfire	7/14/2004	41	1421-2529	

Evergreen forest
Shrub/scrub
Grassland/herbaceous

among the most widely used change point detection methods in hydroclimatological studies (Mallakpour and Villarini, 2016; Zhou et al., 2019). Results for each pixel group (burned, unburned, all pixels) were compared at each basin.

2.4.1.2. Streamflow. The same procedures and tests applied to the ETa data were applied to 'climate-unadjusted' monthly meteorologic (precipitation, air temperature, ETp, SPI) and streamflow (baseflow, runoff) data for continuity. Center of volume analysis was also conducted on the raw streamflow data (daily mean discharge depth) to test for post-fire shifts in streamflow timing. For each water year, the *FlowScreen* R package (Dierauer and Whitfield, 2019) was used to identify the calendar day that 25, 50, and 75 % of the total annual streamflow volume occurred. Pre and post-fire results were compared with Wilcoxon rank sum tests ($\alpha = 0.05$).

In addition, fire-induced shifts in monthly and annual 'climate-adjusted' baseflow and runoff data were quantified. Regression models were fit to annual meteorologic and discharge data and model residuals in the pre and post-fire periods were compared. Separately, monthly data were evaluated by fitting lagged linear regression models to monthly meteorologic and discharge data with a seasonal autoregressive integrated moving average (S-ARIMA) modeled-error term. Model residuals in the pre and post-fire periods were again compared.

3. Multivariate regressions on annual time series

Linear regression models were constructed to estimate annual pre-fire baseflow and runoff from meteorological predictor variables (total annual precipitation, maximum annual daily air temperature, total annual ETp, mean annual SPI ranking). To select the most robust model, regressions for all possible combinations of the four predictor variables were fitted to each response variable (baseflow, runoff). To ensure models made physical sense, any model with a negative precipitation regression coefficient was removed. The model with the lowest cumulative Akaike Information Criteria (AIC) and Bayesian Information Criteria (BIC) score was selected and model validity and accuracy were recorded with model adjusted R^2. Because each annual regression model was constructed with relatively few data points, model residuals for the training data period (pre-fire) were visually inspected to determine if linear regression modeling assumptions were met, including with 'residuals vs fitted' plots for checking linear relationship assumptions, 'normal Q-Q' plots for examining the distribution of residuals, 'scale-location' plots for checking the homogeneity of variance of the residuals (homoscedasticity), and 'residuals vs leverage' plots for identifying extreme values that may be influencing regression results (SI Figure E, SI Figure F) (STHDA, 2018). No model was constructed for baseflow at Porcupine Ranch because no statistically significant regression model was rendered during the model selection process.

Linear annual ordinary least squares regression models were of the general form:

$$y_{ar} = \beta_0 + \beta_1 X_1 + \beta_2 X_2 + \cdots \beta_n X_n + E \quad (1)$$

where y_{ax} denotes the predicted response variable (annual baseflow or runoff), β are regression coefficients, X are input features (predictor variables), and E are model residuals.

Models were then applied to the entire pre and post-fire baseflow and runoff datasets. Assuming the influence of weather was now removed from each model's residuals, the final output (E) was considered to represent the portion of the streamflow signal that land disturbance was accountable for. Comparisons of the residuals in the pre and post-fire periods were made with Wilcoxon rank sum tests. When a Wilcoxon rank sum test indicated a significant difference in post-fire residuals, the authors ensured that the magnitude of the post-fire residual exceeded the magnitude of the predictive model's RMSE.

4. Multivariate lagged regressions on monthly time series

A similar procedure was used to construct regressions on monthly data (same predictor and response variables). To account for seasonal lag between meteorologic predictors and discharge, lagged predictor variables were allowed inclusion in the monthly regression models. This decision was based on the high percentage of precipitation that falls as snow in numerous study basins (Table 1) and the obvious lag between when the majority of precipitation falls and peak runoff occurs in most study basins (SI Figure D). When a predictor variable was significantly correlated with a response variable at multiple lag steps, each lagged version of the predictor was evaluated during the model selection procedure. S-ARIMAs were then fit to the residuals of the lagged linear regression models to remove the explanatory power of any remaining internal autocorrelation (Box and Jenkins, 1976). No models were constructed for baseflow or runoff at Unnamed because no statistically significant regression models were rendered during the linear model selection process.

Lagged linear monthly regression models were of the general form:

$$y_{mx} = \beta_0 + \beta_1 X_{1(t-i(1))} + \beta_1 X_{1(t-i(n))} + \beta_2 X_{2(t-i(n))} + \cdots \beta_n X_{n(t-i(n))} + (P, D, Q)(p, d, q) + E \quad (2)$$

where y_{mx} denotes the predicted response variable monthly baseflow or runoff), β are regression coefficients, X are input features (predictor variables), i is the timestep of the lag, P and p are the autoregressive model terms fitted to seasonal and non-seasonal portions of S-ARIMA models, respectively, D and d are the levels of differencing required for the seasonal and non-seasonal portions S-ARIMA models, respectively, Q and q are the moving average model terms fitted to the seasonal and non-seasonal portions of S-ARIMA models, respectively, and E are S-ARIMA model residuals.

A detailed description of the lagged linear model selection procedure and S-ARIMA model parameterization procedure is provided in SI Appendix B. A figure showing the lagged linear model, the linear model's residuals, the S-ARIMA model, and the final S-ARIMA model's residuals for Chippy Mill is provided in the supplemental information to aid conceptual understanding (SI Figure G).

Assuming the influence of weather and any remaining internal autocorrelation was now removed from each model's residuals, the final output (E) was considered to represent the portion of the streamflow signal that land disturbance was accountable for. To simplify interpretation, baseflow and runoff residuals were grouped by season (Winter = December, January, February; Spring = March, April, May; Summer = June, July, August; Fall = September, October, November). Pre and post-fire comparisons were made with Wilcoxon rank sum tests. When a Wilcoxon rank sum test indicated a significant difference in post-fire residuals, the authors ensured that the magnitude of the post-fire residual exceeded the magnitude of the predictive model's RMSE.

4.0.1. Linking fire-attributed streamflow shifts to ETa

Residuals from the annual linear regression models were used to explore statistical relationships between fire-induced streamflow shift and ETa. First, precipitation and ETa anomalies were calculated. For precipitation, the mean of the total annual precipitation for the entire 21-year study period was subtracted from each year. For ETa, the mean of the total annual ETa in the unburned pixels was subtracted from the mean yearly ETa depth of all the pixels in the basin. To normalize the baseflow and runoff residuals, residual anomalies were also calculated by subtracting the mean of the pre-fire period residual from the 21-year residual time series. Baseflow and quickflow residuals were then summed to determine the magnitude of the total landscape-driven streamflow each year.

Pearson's correlations between annual precipitation, ETa, and streamflow residual anomalies were calculated at each basin. The

anomaly with the stronger correlation was considered the dominant driver of the landscape-driven baseflow or streamflow shift. At-a-glance qualitative volume comparisons were also made by plotting the total mean annual fire-induced streamflow with the total mean annual precipitation and ETa anomalies for each of the five-year post-fire periods.

4.0.2. *Relationships between basin characteristics and fire-attributed streamflow shifts*

The annual baseflow and runoff residuals were also used to explore statistical relationships between fire-induced streamflow shifts and various basin characteristics. This was the only analysis that considered data from all ten of the study basins together.

To normalize data across basins, the percent difference in the mean post-fire baseflow and runoff residuals in the first five post-fire years was calculated for each basin (data from post-fire years six through ten were excluded under the assumption that watershed rehabilitation or recovery would be actively underway by the sixth post-fire year). Pearson's correlation was calculated between the basin attributes (e.g., the percent of each basin burned, percent of basin burned at high severity, total drainage area, and others) and the fire-induced streamflow percent shifts ($\alpha = 0.10$ due to small sample size).

5. Results

5.1. *Fire-induced ETa shifts*

One basin exhibited moderate evidence (p less than 0.05) of a long-term trend in monthly precipitation (Waterfall), one in PET (Ponil Complex), three in SPI (Cannon, Ponil Complex, Waterfall), and two in the ETa of the unburned pixels (Unnamed, Waterfall) according to Mann Kendal trend tests (SI Table A). However, every time series had visually obvious seasonal patterns (SI Figure B, SI Figure C) and failed ADF tests ($p > \alpha$, where $\alpha = 0.05$) when ADF tests were run on raw datasets (prior to the deseasoning procedure). ADF tests indicated that a deseasoning procedure rendered all datasets stationary (SI Table B). The burned-pixel and aggregate basin-scale ETa, baseflow, and runoff datasets were similarly deseasoned, and only the deseasoned baseflow data at Cannon, Ponil Complex, Porcupine Ranch, and Unnamed basins failed the ADF stationarity tests (Fig. 2A and 2B).

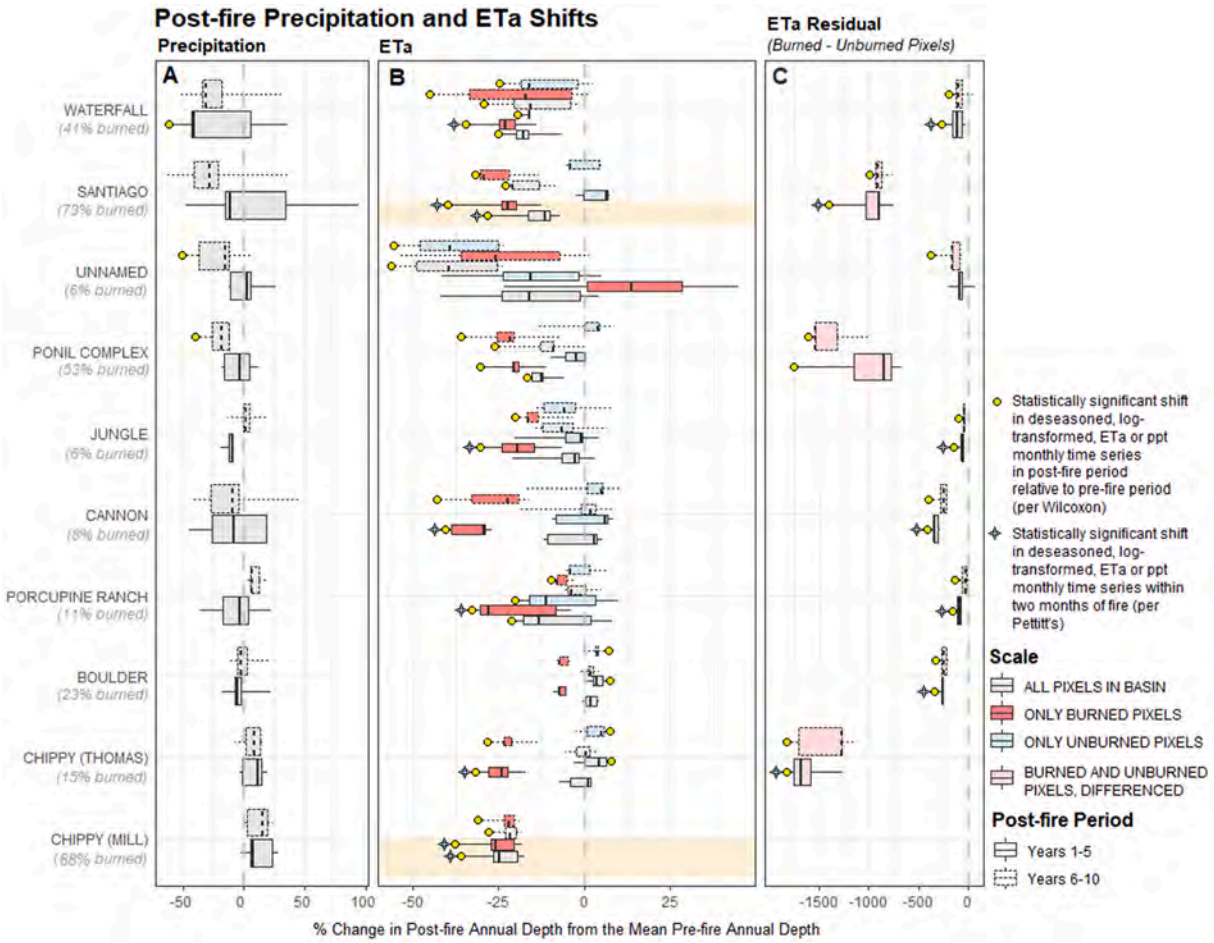

Fig. 3. Boxplots of % change in annual precipitation (A), ETa (B), and the difference (residual) in the ETa of burned and unburned pixels (C) at each basin during the first five and second five post-fire years relative to the pre-fire period (ten years preceding fire). The ten study basins (y-axis) are presented in ascending order of the mean percent change in annual precipitation during the entire post-fire period (post-fire years one through ten) (panel A). The middle panel (panel B) shows shifts in the ETa of burned pixels, unburned pixels, and all pixels within the basin. Significant differences in monthly deseasoned, log-transformed time series in each post-fire period (relative to the pre-fire period) were evaluated with Wilcoxon Rank Sum tests (significance indicated with a yellow dot, $\alpha = 0.05$; deseasoned datasets were not normally distributed according to Shapiro-Wilk normality tests). Dates of significant shifts in the monthly deseasoned data were evaluated with Pettitt's change point detection tests, where a dataset with a significant shift within two months of the fire origin date is indicated with a purple star ($\alpha = 0.05$). Chippy (Mill) and Santiago are highlighted because they were the only basins that experienced significant shifts in ETa within two months of the fire at both the burn scar (burned pixels) and basin scales (all pixels in basin) according to Pettitt's tests. Boxplot center bars indicate median, boxplot hinges are 25th and 75th percentiles, and whiskers are the largest values less than 1.5*IQR (interquartile range) ± each hinge. (For interpretation of the references to colour in this figure legend, the reader is referred to the web version of this article.)

Precipitation during the first five post-fire years was only significantly different (lower) from the pre-fire period at Waterfall according to Wilcoxon rank sum tests (Fig. 3). However, ETa was significantly reduced within most burn scars (burned pixels) in the first five post-fire years (percent annual reductions between approximately ten to 50 %), and in a smaller fraction of burn scars during post-fire years six through ten (likely due to vegetation recovery). The Unnamed fire was the only basin to experience no significant change in post-fire ETa at the burned pixels; this was also the only fire with grassland/herbaceous cover as its dominant pre-fire vegetation type (Table 1). Post-fire ETa residuals (ETa of burned and unburned pixels, differenced) were significantly reduced in every basin during both post-fire periods except at Unnamed (differencing was not performed for Chippy Mill due to its relatively small number of unburned pixels) (Fig. 3C, Fig. 4). Statistically significant post-fire shifts also occurred in baseflow and runoff at numerous basins (Fig. 5), however, the shifts could not be specifically attributed to fire because the influence of climate could not be removed from the gage data. According to the center of volume analysis, the only basin to experience a significant shift in streamflow timing was Chippy Thomas; 25 % of the annual total streamflow volume occurred 21 days later in the first post-fire period. It is not clear whether the shift was caused by land disturbance or post-fire weather as the center of volume analysis was conducted on climate-unadjusted data.

No shifts were detected ($p > \alpha$) in the climate variables (SI Table C) or the ETa of the unburned pixels (Fig. 3B) within six months of a fire origin date according to Pettitt's change point detection tests. Conversely, Pettitt's identified significant shifts in the ETa of the burned pixels within two months of fire origin dates in four of the ten basins

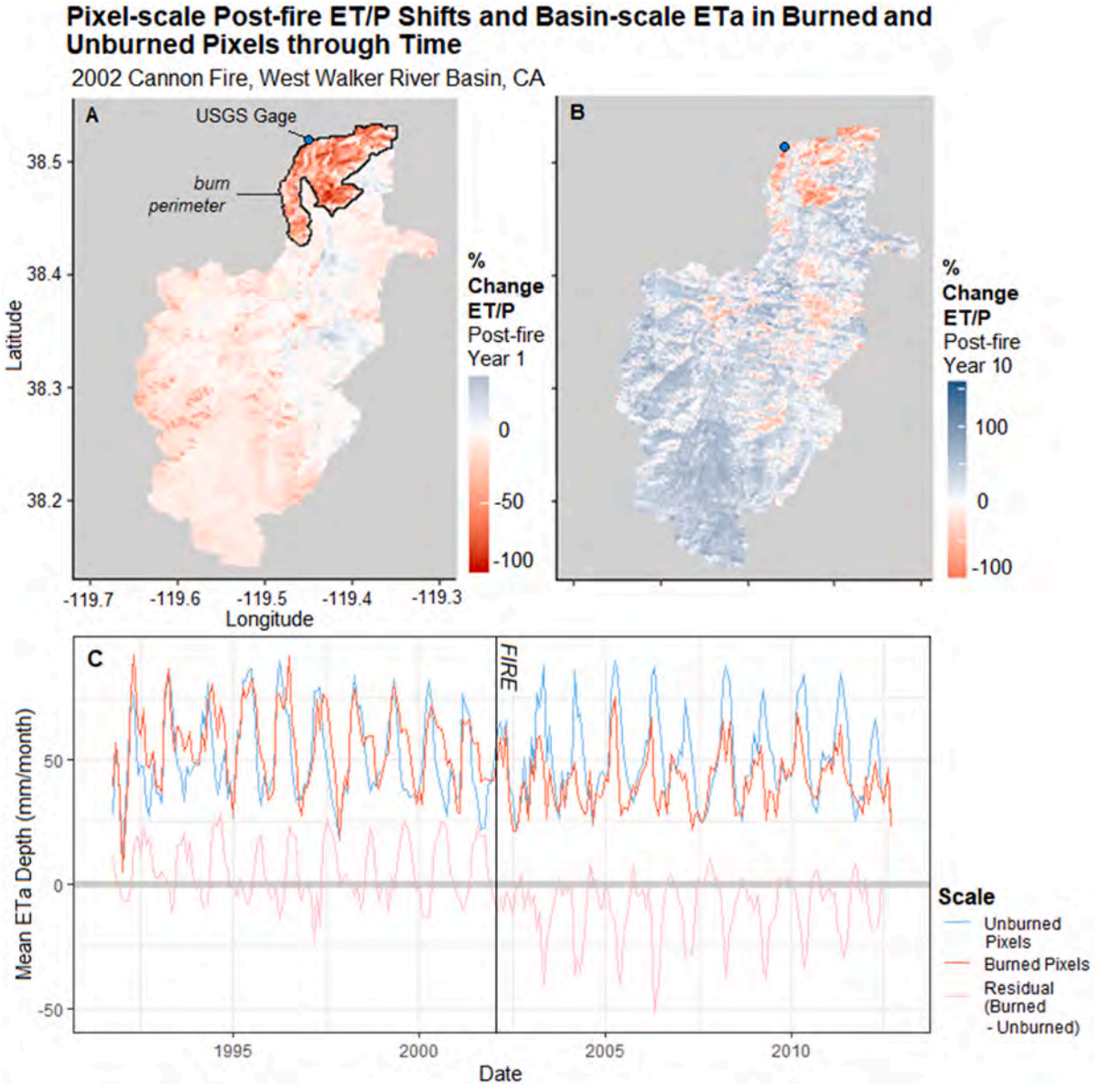

Fig. 4. Post-fire annual evaporation ratio (ET/P) shifts in the first (A) and tenth (B) post-fire years, and monthly ETa through time (C), at the West Walker River Basin, California, following the 2002 Cannon Fire. Panels A and B: ET/P percent shifts are the percent shift in the annual evaporation ratio at each pixel relative to each pixel's ten-year pre-fire evaporation ratio. Reductions in the post-fire ratio (relative to the pre-fire) shown in red-scale, increases are shown in blue-scale. Approximate location of the USGS stream gage is indicated with a blue dot. Panel C: The mean monthly ETa depth through time for all unburned pixels in the basin (blue line), all burned pixels in the basin (red line), and the difference between the burned and unburned pixels (pink line, with an obvious reduction occurring following the fire event). Approximate date of the fire is indicated with a vertical black line. (For interpretation of the references to colour in this figure legend, the reader is referred to the web version of this article.)

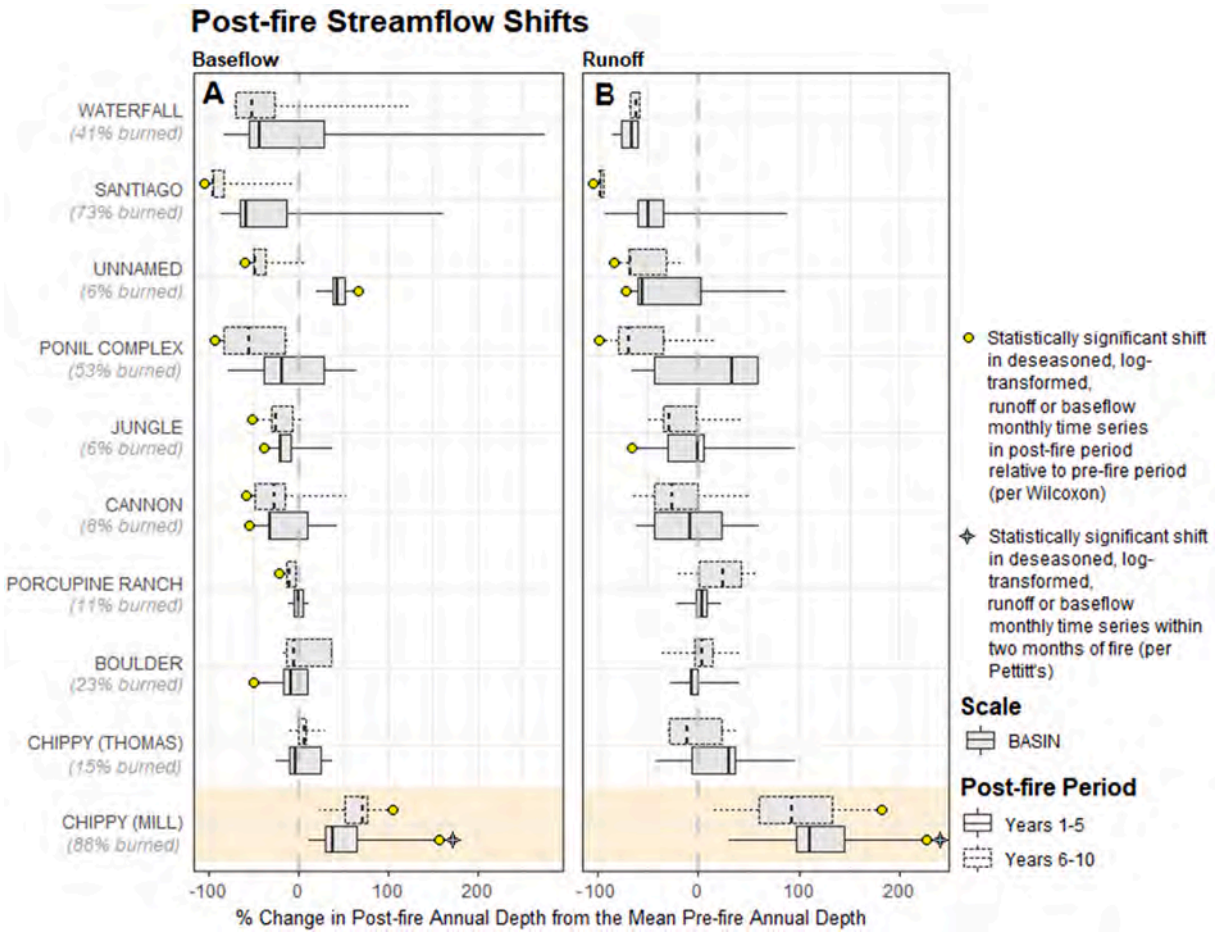

Fig. 5. Boxplots of % change in annual baseflow (A) and runoff (B) at each basin during the first five and second five post-fire years relative to the pre-fire period (ten years preceding fire. The ten study basins (y-axis) are presented in the same order used in Fig. 3. Significant differences in monthly deseasoned, log-transformed time series in each post-fire period (relative to the pre-fire period) were evaluated with Wilcoxon Rank Sum tests (significance indicated with a yellow dot, $\alpha = 0.05$). Dates of significant shifts in the monthly deseasoned data were evaluated with Pettitt's change point detection tests, where a dataset with a significant shift within two months of the fire origin date is indicated with a purple star ($\alpha = 0.05$). Chippy (Mill) is highlighted because it was the only basin that experienced a significant shift in baseflow and/or runoff during the water year proceeding the year of the fire according to Pettitt's tests. Boxplot center bars indicate median, boxplot hinges are 25th and 75th percentiles, and whiskers are the largest values less than 1.5*IQR ± each hinge. (For interpretation of the references to colour in this figure legend, the reader is referred to the web version of this article.)

(Chippy Thomas, Chippy Mill, Porcupine Ranch, Santiago) and within five months of fire origin dates for three additional basins (Cannon, Jungle, Waterfall). Significant shifts occurred in the ETa residuals of those same seven basins within two months of fire origin dates (Fig. 3C, SI Table C). Comparison of the burned pixel and 'all pixel' ETa Pettitt's results provides insight into the effect of scale: significant shifts in the ETa of all basin pixels were only identified within two months of fire origin dates at the two basins with the highest percentages of burned drainage area (Chippy Mill – 88 %, Santiago – 73 %) (Fig. 3B). Chippy Mill was the only basin to experience significant baseflow and runoff shifts during the water year following the fire (Fig. 5).

5.2. Fire-induced streamflow shifts

5.2.1. Annual shifts

Based on comparisons of pre and post-fire residuals from the annual regression models, statistically significant fire-induced increases in baseflow were identified at Chippy Mill (68 % increase from pre-fire annual baseflow, or approximately 30-mm/year) and Unnamed (53 % increase, approximately 5-mm/year) (Fig. 6A) during the first five post-fire years (detailed model metrics provided in SI Table D). Of the three basins with statistically significant increases in baseflow during post-fire years one through five, significant increases only persisted into post-fire years six through ten at Chippy Mill (Fig. 6B). Statistically significant immediate increases in annual runoff were identified at Cannon (8 % increase, approximately 25-mm/year) and Chippy Mill (99 % increase, approximately 95-mm/year). That increase only persisted at Chippy Mill (92 % increase) during the second post-fire period (Fig. 6B).

During the first five post-fire years, wildfire increased average annual flow by 6 % Cannon, 43 % at Chippy Mill, 2 % at Jungle, 23 % at Ponil Complex, and 8 % at Waterfall (red text in Fig. 6). Wildfire decreased flows by 1 % at Boulder, 87 % at Santiago, and 9 % at Unnamed. These changes are likely within the range of pre-fire interannual streamflow variability where comparisons of pre and post-fire model residuals were insignificant (absence of a yellow dot in Fig. 6).

5.2.2. Seasonal shifts

Analysis of annual hydrologic data did not capture the most dramatic and seasonally acute fire-induced streamflow shifts. Nearly every basin experienced increased mean and median baseflow and runoff in some seasons and decreases in others (Fig. 7) (detailed model metrics provided in SI Table E). We observe that the seasonal timing of fire-induced baseflow increases and decreases did not have a consistent temporal relationship with seasonal precipitation across basins. For example, at Chippy Mill and Cannon, which receive 43 and 72 % of their annual average precipitation as snow, respectively (Table 1), fire increased

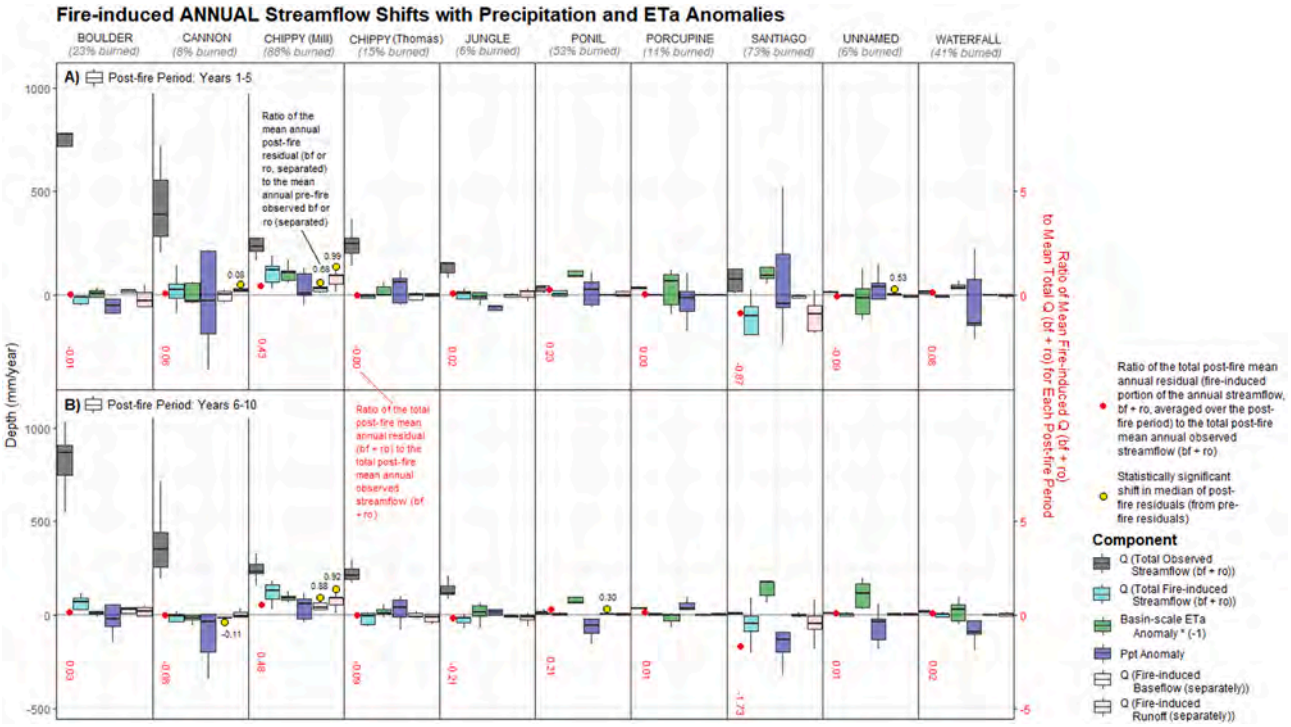

Fig. 6. Fire-induced yearly baseflow (white boxes) and runoff shifts (pink boxes) with precipitation (dark blue boxes), ETa anomalies (green boxes), and total annual observed streamflow (grey boxes) during the first five (A) and second five (B) post-fire years. The 'fire-induced' shifts are the residuals from the annual regression analysis (discussed in section 3.2.1). Significant shifts in the residuals of the post-fire period, relative to the residuals of the pre-fire period, were evaluated with Wilcoxon rank sum tests (significance indicated with a yellow dot, $\alpha = 0.10$). The black text above or below a yellow dot is the ratio of the post-fire residual to the average annual pre-fire observed baseflow or runoff. For example, in panel A, fire significantly increased runoff at the Cannon Fire by 8 % relative to the mean annual volume of pre-fire runoff. In addition, to enable at-a-glance comparisons of the amount of water made available from yearly precipitation and ETa anomalies to the amount of fire-boosted streamflow, the total fire-induced streamflow (sum of the annual baseflow and runoff residual) is plotted as turquoise boxes next to the magnitude of the precipitation and ETa anomalies; note that the ETa anomaly was multiplied by −1 to aid comparison. The ratio of the mean annual fire-induced streamflow (baseflow plus runoff residual) to the mean annual observed total post-fire streamflow is provided in red and plotted with a red dot (corresponding to the right y-axis). For example, at the Cannon Fire, fire-induced streamflow comprised 6 % of the total annual streamflow observed at the gage in the post-fire period. Boxplot center bars indicate median, boxplot hinges are 25th and 75th percentiles, and whiskers are the largest values less than 1.5*IQR ± each hinge. (For interpretation of the references to colour in this figure legend, the reader is referred to the web version of this article.)

baseflow during wet months (mean monthly hydrologic fluxes provided in SI Figure D)). The opposite occurred at Oregon's Boulder fire (20 % of annual precipitation falls as snow), where baseflow increased during the dry summer and fall months and decreased during the wetter winter and spring months. The Oregon results were in agreement with Bart and Tague (2017)'s observations of burn scars in central and southern California (where similarly low to no persistent winter snow accumulates), where lower post-fire groundwater ETa losses likely caused baseflow to increase during the dry months. While the effect of forest disturbance on snowpack is influenced by numerous factors, vegetation removal and fire-induced radiative forcing have generally been shown to advance the date of snow disappearance by increasing snowmelt rates (Gleason et al., 2013; Gleason and Nolin, 2016; Pomeroy et al., 2012; Pugh and Gordon, 2013; Skiles and Painter, 2015). Earlier post-fire snowmelt may have contributed to decreased baseflows during the drier summer months at Chippy Mill and Cannon.

Only Chippy Mill experienced statistically significant, seasonally opposed baseflow shifts (increases in some seasons, decreases in others) during the first five post-fire years, (49 % increase in spring, or approximately 3-mm/month;17 % decrease during fall, approximately 2-mm/month). This may be because fire-induced baseflow increases overlapped with the peak precipitation season in most basins (when precipitation likely varies the most during any given water year). This is further supported by the observation that at many basins, wet season precipitation variability was high between water years (SI Figure A), which increased the variability of the landscape-driven baseflow residuals for the wetter months during the pre-fire period. Therefore, at most basins, fire-driven baseflow increases (typically occurring in the wetter months) were less likely to be statistically insignificant compared to baseflow reductions (which often occurred during the drier months, when interannual precipitation variability was lower).

The same pattern was observed in the runoff results: only Chippy Mill experienced statistically significant, seasonally opposed runoff shifts during the first five post-fire years. Numerous additional basins experienced statistically significant shifts in runoff during the first five post-fire years in at least one season (Boulder: reductions in winter and summer; Cannon: increases in fall; Chippy Thomas: decreases in winter; Jungle: increases in winter; Ponil Complex: increases in winter and spring; Santiago: decreases in summer) (Fig. 7B). Only Chippy Mill (88 % burned) and Santiago (73 % burned) experienced significant runoff shifts during the second post-fire period (Fig. 7C and D).

5.3. Linking fire-attributed streamflow shifts to ETa

Chippy Mill was the only basin whose fire-induced streamflow shifts were well-explained by ETa (R^2 = -0.79) (Fig. 8). Shifts were also significantly correlated with the precipitation anomaly, but to a lesser extent ($R^2 = 0.14$). Also at Chippy Mill, qualitative comparisons of total annual fire-induced streamflow depth (turquoise boxplots) to the depth of water expected from basin-scale ETa anomaly (green boxplots) and precipitation anomaly (blue boxplots) shows that the ETa anomaly was nearly equivalent (opposite) in magnitude to the fire-induced annual streamflow depth during each of the post-fire periods (Fig. 6). Conversely, the depth of excess water provided by the precipitation

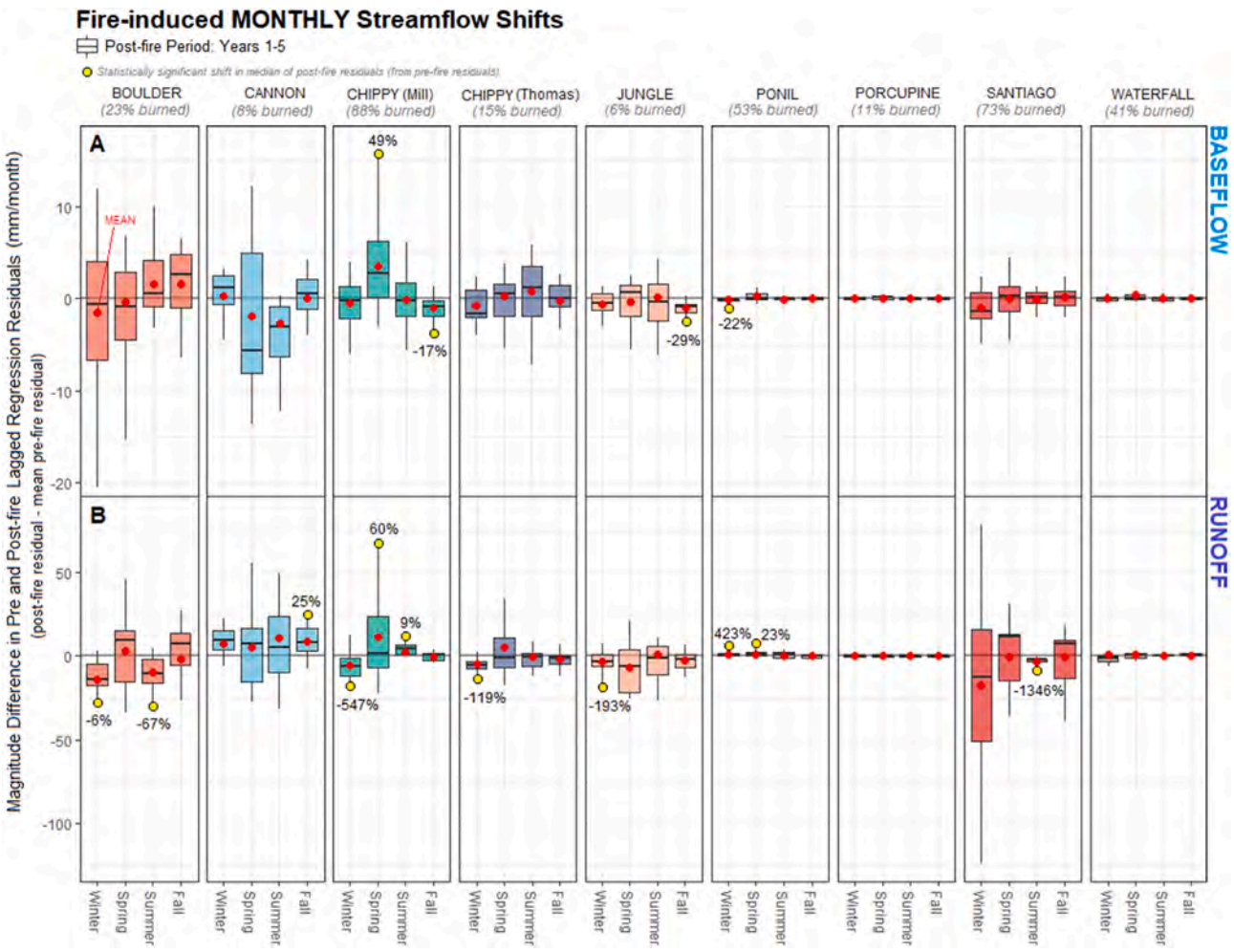

Fig. 7. Fire-induced monthly baseflow and runoff shifts during the first five (A, B) and second five (C, D) post-fire years. Each boxplot represents five data points, where a data point is the difference in the mean of the residual for all three months in the season relative to the mean of the residuals from the same three months for the entire ten-year pre-fire period. Significant shifts in the residuals of the post-fire period, relative to the residuals of the pre-fire period, were evaluated with Wilcoxon rank sum tests (significance indicated with a yellow dot, $\alpha = 0.10$). For example, during spring at Chippy Mill, wildfire increased runoff by 60 % in the first five post-fire years (panel B). Boxplot center bars indicate median, red dots indicate mean, boxplot hinges are 25th and 75th percentiles, and whiskers are the largest values less than 1.5*IQR ± each hinge. (For interpretation of the references to colour in this figure legend, the reader is referred to the web version of this article.)

anomaly was insufficient to account for the total annual fire-induced streamflow depth. This further supports our hypothesis that much of Chippy Mill's post-fire boosted streamflow was surplus water generated by fire-induced ETa reduction.

Although ETa reductions occurred at most of the other burn scars (Figs. 3 and 6), landscape-driven streamflow could not be statistically linked to the ETa or precipitation signal. This may indicate that where fire caused streamflow to increase, other fire-modified landscape processes also contributed to increased precipitation-runoff partitioning (e.g., reduced infiltration (DeBano et al., 1998)). Further explanation may be provided by plots of annual evaporation ratios and aridity indices (SI Figure H): every watershed was water-limited during most years except Oregon's Boulder basin, meaning some or all of the excess water generated from ETa reduction could have been consumed by various compensation pathways, such as through compensatory transpiration losses by intact hillslope and riparian vegetation within and downstream of the burn scar (Tague et al., 2019). This hypothesis highlights the potential importance of unburned drainage area positioned between the disturbance footprint and the basin outlet (discussed below) or unburned riparian vegetation within the burn scar. In addition, our data show that some basins had evaporation ratios greater than 1.0 during multiple years, suggesting that ETa fluxes may be supported by additional inputs of water beyond precipitation (e.g., deep groundwater reserves) (Sun et al., 2019; Vourlitis et al., 2008). We also note that many basins have lower interannual ETa variability than precipitation variability, indicating that ETa water sources are appreciably distinct in space and time from streamflow water sources (i.e., hydraulically disconnected at timescales relevant to interannual ETa flux) (SI Figure A). Further studies are needed to determine how wildfire modifies runoff generation processes in different lithologic typologies.

5.4. Relationships between basin characteristics and fire-attributed streamflow shifts

Numerous Pearson's correlations greater than 0.20 were calculated between fire-induced baseflow and runoff shifts and select basin attributes (Table 2). Likely due to small sample size, only correlations greater than or equal to 0.58 were statistically significant.

Greater amounts of burned area, area burned at high severity, and the percent of a basin impacted by beetles prior to fire significantly correlated with fire-induced runoff increases. The percent of total precipitation that falls as snow, slope, and depth to a restrictive layer also correlated positively with fire-induced increases in runoff, although not statistically significantly. The average annual aridity index was

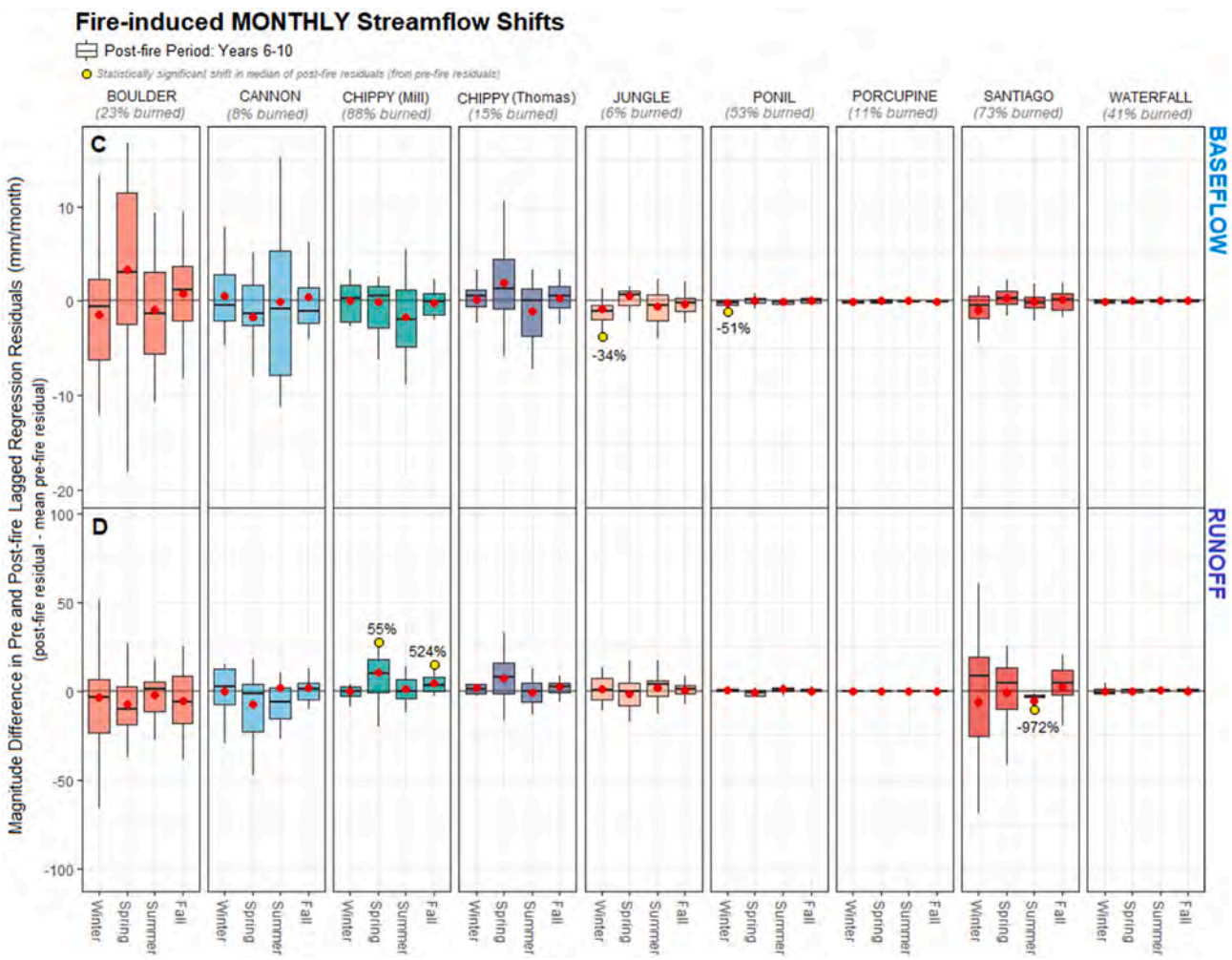

Fig. 7. (*continued*).

significantly positively correlated with fire-induced baseflow increases; slope was significantly negatively correlated with fire-induced baseflow increases.

6. Discussion

6.1. Identifying ETa-induced streamflow modification following wildfire disturbance at the gage

Only when at least 73 % of a basin burned in a single water year was moderate evidence present of fire-induced ETa shifts (p less than 0.05, Wilcoxon rank sum tests) in basin-scale ETa data summaries (Fig. 3). Downstream, only where basin-scale ETa was significantly altered within two months of the fire were fire-induced streamflow shifts distinguishable at the gage without prior removal of the climate signal according to Pettitt's tests (Chippy Mill, 88 % burned, Fig. 5). These findings highlight the importance of disturbance scale and are further bolstered by strong correlations between the magnitude of fire-induced runoff shifts and the percentage of total burned contributing drainage area (Table 2). Previous work confirms the sensitivity of streamflow to the fraction of drainage area disturbed (Hallema et al., 2018; Saxe et al., 2018; Williams et al., 2022; Wine et al., 2018).

We show that the amount of fire-induced runoff generated from the Chippy Mill burn scar (the basin with the highest percentage of disturbed contributing drainage area) was proportionate to the depth of water made available by fire-induced ETa reduction (Fig. 6). This suggests that, where the majority of a basin is disturbed, inferences can be made about post-fire runoff response from pixel-scale ETa data. However, mixed results from the other nine basins suggest the following five points be considered when using basin-scale data in change detection analysis:

First, if basin-scale data (e.g., stream gage data) are expected to relay the story of landscape disturbance, the tendency for post-fire climate to mask or artificially exaggerate the effect of landscape disturbance in the basin-scale dataset should be accounted for. Only where nearly the entire basin burned (Chippy Mill) were fire-induced streamflow shifts extreme enough to be identified with climate-unadjusted statistical methods (Pettitt's tests on deseasoned monthly data). In the other basins included in this study, climate-unadjusted streamflow followed the declining precipitation pattern (Figs. 3A, 5). This supports Jaramillo and Destouni (2014)'s observation that landscape drivers often cause hydrologic processes to shift in a direction opposite to those imposed by atmospheric climate drivers. Hallema et al. (2018) confirmed it when they observed a net decline in post-fire streamflow following reduced post-fire precipitation in southern and central California. Blöschl et al. (2007) tied this concept back to total basin size when they observed that large-scale climatic patterns dominate the hydrologic response of large watersheds more so than in small watersheds, thus the effects of wildfire disturbance are more likely undetectable in comparatively large basins (Blöschl et al., 2007).

Second, because fire-induced streamflow shifts were seasonally variable (Fig. 7), even climate-adjusted procedures are liable to miss the most acute effects of fire when data are aggregated to the annual timestep because the effects of the disturbance may be averaged out. Our

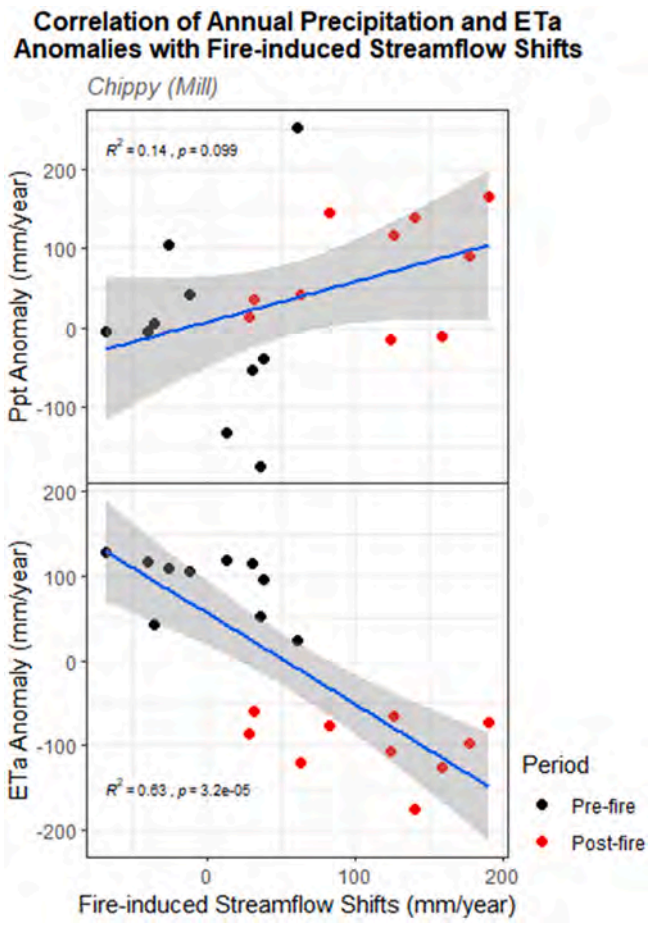

Fig. 8. Pearson's correlation of annual precipitation (Ppt) and ETa anomalies with the portion of annual streamflow not explained by meteorologic variables at Chippy Mill in the pre-fire (block dots) and post-fire (red dots) periods. The precipitation anomaly (TOP) is the deviation from the 21-year average annual precipitation, the ETa anomaly (BOTTOM) is the deviation of all the pixels in the basin from the 21-year average of annual ETa in unburned pixels only. Correlations were calculated at all ten study basins but were only significant ($\alpha = 0.10$) at Chippy Mill (results from other basins not pictured). Correlations between streamflow residuals and ETa anomaly of the burned pixels were also calculated (not pictured) but Chippy Mill remained the only basin with significant results. (For interpretation of the references to colour in this figure legend, the reader is referred to the web version of this article.)

finding supports Aredo et al. (2021) process-based modeling study of the effects of land use/land cover change on seasonal discharge in Ethiopia: mean monthly streamflow decreased during dry months and increased during wet months following conversion of forested and bushland areas to urban and agricultural land uses (Aredo et al., 2021).

Third, our lagged monthly regression residuals still loosely tracked meteorology in the post-fire period. This may partially explain why post-fire shifts were frequently insignificant when results were aggregated into five-year blocks – the magnitude, and for some basins the direction, of the fire-induced streamflow shifts varied from year to year (Figs. 6 and 7). The Chippy Thomas basin (15 % burned by a fire in 2007) illustrates the point well: annual fire-attributed streamflow shifts were plotted with precipitation anomaly, ETa anomaly, and the status of each year's annual SPI ranking (above, within, or below the 95 % confidence interval (CI) of the entire 21-year SPI median score) (Fig. 9). At the annual timestep, the direction of 'fire-induced' baseflow and runoff shifts still generally followed the direction of the precipitation anomaly; it was not until the fourth post-fire year (2011) that the fire-induced portion of the total annual streamflow depth became substantially elevated – the same year the basin received above-average precipitation for the first time since the fire year (per SPI rank). Overall, this suggests that even if a robust statistical method is used to remove climate from the streamflow record, the nuanced effects of multi-year drought or wetness on runoff generation processes are not well-accounted for; there may be a 'catchment memory' of drought. For example, it has been shown that 'drought history' is more important than real-time antecedent soil moisture status for infiltration and water repellency behavior in forested areas (Gimbel et al., 2016).

Fourth, the assumption that our procedures isolated *fire*-induced streamflow shifts specifically introduced uncertainty. Numerous additional landscape drivers are capable of modifying watershed hydrology such as insect infestation, disease, drought-induced vegetation mortality, and anthropogenic activities such as land cover conversion and water extraction from surface or groundwater reservoirs (Jaramillo and Destouni, 2014; Xu et al., 2014). We attempted to limit that uncertainty by selecting relatively unpopulated basins with natural flow regimes (Wine and Cadol, 2016). Regarding our attempt to link fire-induced streamflow shifts to ETa reduction specifically, we acknowledge that combustion modifies myriad hydrogeomorphological processes, only some of them participatory in ETa regulation. For example, some studies have observed fire-induced soil infiltration impedance to be a dominant driver of post-fire runoff generation at plot and hillslope scales (Balfour et al., 2014; Ebel et al., 2012). Event-specific storm characteristics and initial soil–water saturation deficit have also been shown to modulate peak runoff rates in fire-affected soils (Moody and Ebel, 2014). Fire-exacerbated geomorphological processes (debris flows, dry raveling, etc.) also likely alter runoff routing parameters (e.g., hillslope, floodplain, and channel surface roughness; side-channel storage) (de Haas et al., 2014; Florsheim et al., 2016). We verified that fire reduced ETa *before* assuming ETa played a role in what occurred at the gage but admit that some or all aforementioned processes also likely contributed to the expression of landscape disturbance in the streamflow record. See also (Kirchner et al., 2020) for further discussion of ETa's controlling role in streamflow response following forest density reduction.

Finally, our results suggest that the period length streamflow data are aggregated to may partially determine the disturbance percentage threshold necessary to confer a detectable shift in gage data. Perhaps in part due to our consideration of all seasons, the current work identified significant fire-induced streamflow shifts in basins with as little as 6 % burned contributing drainage area. In contrast, Hallema et al. (2018) and Wine and Cadol (2016) procedures detected fire-induced annual or monsoonal runoff increases in basins with at least 19 % burned drainage area. Future work could explicitly quantify streamflow's elasticity to fire-induced ETa modification (Hallema et al., 2018; Kurzweil et al., 2021).

6.2. *Watershed factors promoting fire-induced streamflow shifts*

Results from the current study support prior observations that the percentage of total burned and high burn severity drainage area controls the magnitude and direction of the streamflow modification (Blöschl et al., 2007; Neary et al., 2005; Saxe et al., 2018; Williams et al., 2022; Wine and Cadol, 2016). For one, high burn severity has been shown to reduce ETa more dramatically and for longer durations (Collar et al., 2021; Ma et al., 2020; Nolan et al., 2014; Poon and Kinoshita, 2018). More high burn severity area also decreases the chances for compensatory increases in transpiration or evaporation from the soil, the understory, or neighboring or downgradient vegetation (Tague et al., 2019). Similarly, less unburned drainage area reduces the opportunities for intact, downgradient vegetation to consume excess water generated by the upslope ETa reduction (Goeking and Tarboton, 2020; Tague et al., 2019). The fraction of burned drainage area may have also been a proxy for watershed size in our data, as larger watersheds are at decreased risk of experiencing synchronous, basin-wide, stand-replacing disturbance. And due to rainfall's inherent spatial variability, the percentage of a watershed's area that is likely to generate runoff at any given time is

Table 2
Pearson's correlation between select basin attributes and the fire-attributed percent shift in baseflow and runoff (according to the annual regression method discussed in section 3.2.1). Blank cell indicates a correlation coefficient smaller than ± 0.20. Statistically significant correlations (α = 0.10) are underlined.

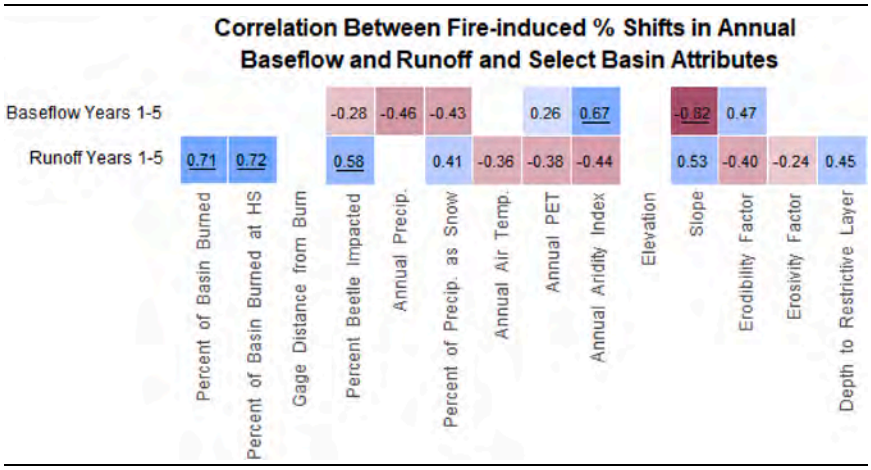

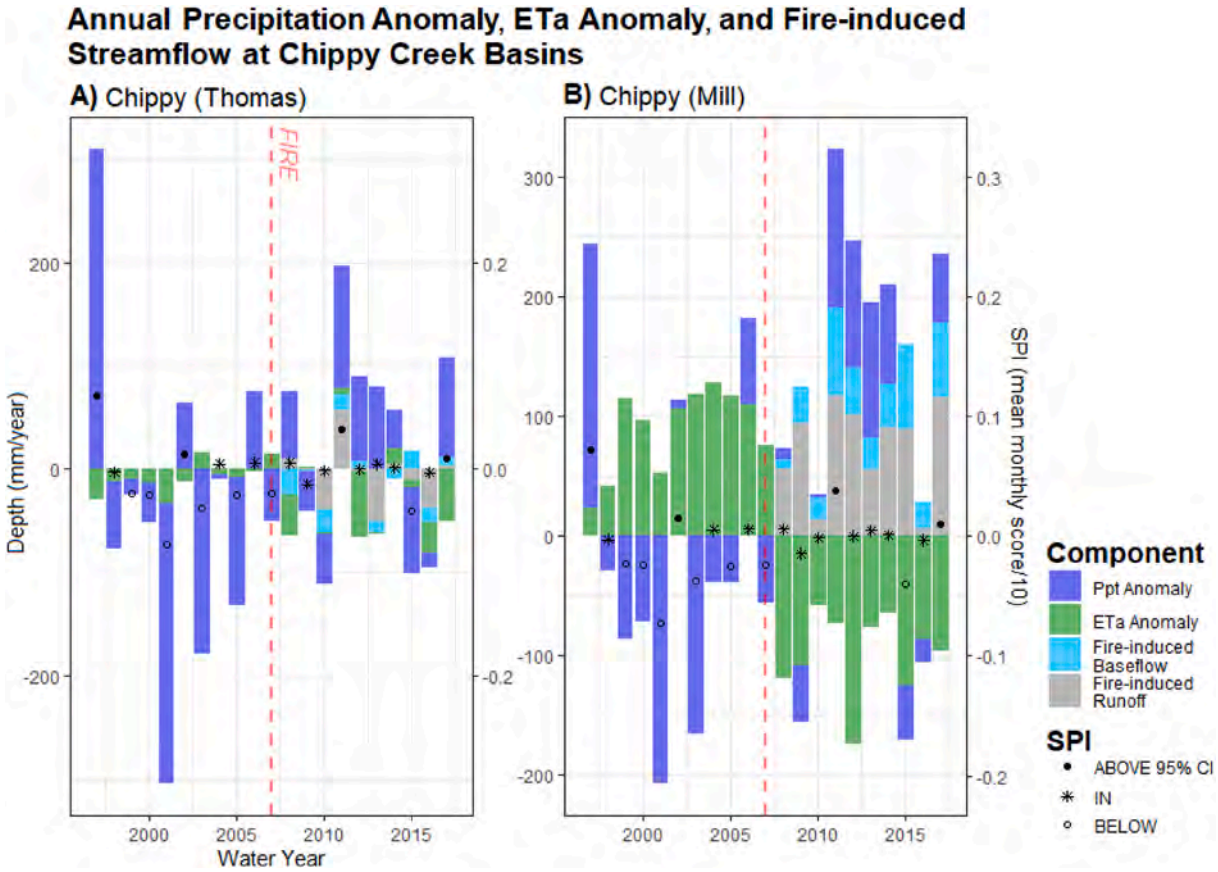

Fig. 9. Annual precipitation (Ppt), ETa, Standardized Precipitation Index (SPI) anomalies, and fire-induced baseflow and runoff at Chippy Thomas and Chippy Mill. The SPI symbol provided in legend indicates if the annual SPI score was above, within, or below the 95% CI of the entire 21-year mean SPI score for the basin. SPI score is divided by ten for plotting purposes (right y-axis). Fire year indicated with red dashed vertical line.

inversely related to its size (Brunkal and Santi, 2017). Finally, the specific effect of any one particular perturbance is difficult to verify at large spatial scales because of the long time lag between cause and effect (Blöschl et al., 2007).

The lateral distance from the gaging station to the closest burn perimeter was not significantly correlated with fire-induced baseflow or quickflow (Table 2). These results do not support the prior observation that the position of a disturbance in the landscape matters (Blöschl et al., 2007) as longer channel lengths increase the opportunity for peak flow attenuation (Brunkal and Santi, 2017; Ffolliott et al., 2013; Mueller et al., 2010). However, our results do not deliver strong evidence to the contrary given the relatively small sample size and annual timestep of our data and the variability in disturbance severity across the ten study basins. It is also reasonable to assume that opportunities for down-gradient compensatory ETa losses are fewer as the area between the disturbance and the basin outlet gets smaller (Tague et al., 2019).

6.3. Implications for surface water resources

We studied a range of spatiotemporal scales to determine when fire-induced hydromodification becomes relevant to source-water hydrology. However, we appreciate Bloschl et al. (2007)'s cogent reminder that the spatial scale at which land cover change can impact overall basin hydrology depends on the hydrologic setting. Our paucity of replicates and the relatively sparse number of hydrologic settings evaluated limits our ability to issue broad, general statements about the western United States from the current work. Future efforts could increase the number or study basins by installing temporary pressure transducers where data are desired but no USGS gaging stations exist. For example, see Lundquist et al., 2005's nested monitoring approach in the Tuolumne River basin.

In basins with unburned adjacent or downgradient drainage area, our results suggest that compensation pathways may have consumed some or all of the excess water generated by ETa reductions. Literature suggests that the seasonal droughts typical of semi-arid and Mediterranean climate regimes, where ETa is often water versus energy-limited during peak ETa months, are likely to enhance the conditions that support these compensation pathways (Tague et al., 2019). The authors acknowledge that we were unable to compare our results with energy-limited basins as our study areas were generally water-limited (SI Figure H). For now, previous publications can be visited for regional-scale statements about the effects of wildfire on streamflow (Beyene et al., 2021; Hallema et al., 2018; Saxe et al., 2018; Williams et al., 2022). For example, Hallema et al. (2018) found that wildfire boosted annual discharge at study sites in the Pacific Northwest, Texas-Gulf, and lower Colorado regions, while the southeastern United States and areas treated with prescribed fire were relatively unaffected.

We do show that where the majority of the drainage area was unburned, the magnitude of fire-induced hydromodification was often within the range of pre-fire interannual streamflow variability (Figs. 6 and 7) or was relatively transient. This may suggest that water providers with large, diverse water supply portfolios are insulated from post-fire water budget modification. Conversely, water providers with small source-water collection areas are at greater risk because they are more likely to experience disturbance in a larger fraction of their collection area. Thus, pre-fire management strategies that reduce the risk of moderate to high burn severity, expand source-water area, or diversify water supply portfolios may be most important for small-scale water providers. In addition, where climatic and fuel conditions favor fire and multiple ignition sources are present, land managers should consider the additive effect of multiple fire events (Wine and Cadol, 2016).

7. Conclusions

We evaluated whether fire-induced streamflow shifts were caused by changes in burn scar ETa at ten basins in the western United States. Fine resolution ETa was estimated with the SSEBop model at burned and unburned 30-m pixels, which allowed for the effects of climate to be easily separated from landscape disturbance in ETa time series. Fire reduced ETa through the tenth post-fire year at 80 % of the studied burn scars (Fig. 3), however, those reductions were only propagated up to the basin scale when at least 73 % of the basin's drainage area burned in a single water year. Only then were fire-induced streamflow shifts detected in climate-unadjusted streamflow data (Fig. 5).

To remove the influence of climate from the streamflow data, previously proposed methods were used to process annual data and improved upon for monthly data. Fire-induced baseflow and runoff shifts were detected at a basin with as little as 6 % burned drainage area (Fig. 7), representing a substantial improvement in the sensitivity of statistical methods to detect landscape-driven streamflow shifts than what was previously available in the literature. A potential explanation may be the fact that most change detection work is conducted on annual time series, yet the effect of fire disturbance on streamflow magnitude is seasonally variable (Fig. 7). This suggests that the effects of land disturbance on watershed hydrology may be partially averaged out in annual datasets. However, even in the climate-adjusted streamflow data, fire-induced streamflow shifts were generally insignificant or short-lived (did not persist past the fifth post-fire year) (Fig. 7C and D) where burn scar ETa reductions were not propagated up to the basin scale.

Despite fire-induced ETa reductions at most burn scars, post-fire ETa anomalies were only significantly correlated with fire-induced streamflow shifts at the basin with the highest percentage of disturbed drainage area (Chippy Mill, 88 %) (Fig. 8). This may indicate that other fire-modified physical processes contributed to the increased post-fire streamflow observed elsewhere (Fig. 6). Where fire reduced burn-scar ETa but did not increase streamflow, our results support prior findings that in water-limited systems, compensation pathways may develop in adjacent or downgradient undisturbed or low burn severity areas that consume the excess water yielded from ETa reduction.

Overall, findings suggest that water providers with large source-water collection areas are fairly immune to disturbance-induced shifts in basin water yield because they are less likely to experience disturbance in substantial portions of their collection area. For the same reason, providers with relatively small source-water areas are at higher risk and should therefore consider management strategies that reduce the likelihood of high severity disturbances or that expand or diversify water supply portfolios. Results from this study would be bolstered by in situ field observations and process-based modeling studies of the mechanics behind fire-modified precipitation partitioning and runoff routing. The need for additional research into the role of groundwater storage in the post-fire water budget is also highlighted.

CRediT authorship contribution statement

Natalie M. Collar: Conceptualization, Methodology, Data curation, Formal analysis, Visualization, Writing – original draft, Writing – review & editing, Funding acquisition. **Samuel Saxe:** Data curation, Writing – review & editing. **Brian A. Ebel:** Conceptualization, Methodology, Writing – review & editing, Supervision, Funding acquisition. **Kathryn S. Boden:** Conceptualization, Methodology, Writing – review & editing. **Ashley J. Rust:** Conceptualization, Writing – review & editing. **Terri S. Hogue:** Conceptualization, Methodology, Writing – review & editing, Supervision.

Declaration of Competing Interest

The authors declare that they have no known competing financial interests or personal relationships that could have appeared to influence the work reported in this paper.

Data availability

Data are available on USGS ScienceBase at https://www.sciencebase.gov/catalog/item/628e58f9d34ef70cdba3feda.

Acknowledgements

This work was partially funded by the USGS's Water Availability and Use Science Program. Additional support was provided by a Lincoln Institute of Land Policy Babbitt Dissertation Fellowship (C21-021) and a Colorado Association of Stormwater and Floodplain Managers 2021 research grant. All parent data were obtained from public domains and are freely available; detailed source information is provided in Appendix A. Data generated for the study are available online at https://www.sciencebase.gov/catalog/item/628e58f9d34ef70cdba3feda. Any use of trade, firm, or product names is for descriptive purposes only and does not imply endorsement by the U.S. government. The authors thank the editor, associate editor, the three anonymous reviewers, and Dr. David M. Rey of the U.S. Geological Survey, for their valuable comments.

Appendix A. Supplementary data

Supplementary data to this article can be found online at https://doi.org/10.1016/j.jhydrol.2022.128242.

References

Abatzoglou, J.T., 2013. Development of gridded surface meteorological data for ecological applications and modelling. Int. J. Climatol. 33, 121–131. https://doi.org/10.1002/joc.3413.

Aredo, M.R., Hatiye, S.D., Pingale, S.M., 2021. Impact of land use/land cover change on stream flow in the Shaya catchment of Ethiopia using the MIKE SHE model. Arab. J. Geosci. 14, 114. https://doi.org/10.1007/s12517-021-06447-2.

Ault, T.R., 2020. On the essentials of drought in a changing climate. Science 368, 256–260. https://doi.org/10.1126/science.aaz5492.

Bales, R.C., Goulden, M.L., Hunsaker, C.T., Conklin, M.H., Hartsough, P.C., O'Geen, A.T., Hopmans, J.W., Safeeq, M., 2018. Mechanisms controlling the impact of multi-year drought on mountain hydrology. Sci. Rep. 8, 690. https://doi.org/10.1038/s41598-017-19007-0.

Balfour, V.N., Doerr, S.H., Robichaud, P.R., 2014. The temporal evolution of wildfire ash and implications for post-fire infiltration. Int. J. Wildland Fire 23, 733. https://doi.org/10.1071/WF13159.

Bart, R.R., Tague, C.L., 2017. The impact of wildfire on baseflow recession rates in California. Hydrol. Process. 31, 1662–1673. https://doi.org/10.1002/hyp.11141.

Bart, R.R., Tague, C.L., Moritz, M.A., 2016. Effect of Tree-to-Shrub Type Conversion in Lower Montane Forests of the Sierra Nevada (USA) on Streamflow. PLoS ONE 11, e0161805.

Bastiaanssen, W.G.M., Pelgrum, H., Wang, J., Ma, Y., Moreno, J.F., Roerink, G.J., van der Wal, T., 1998. A remote sensing surface energy balance algorithm for land (SEBAL): 2: Validation. J. Hydrol. 212–213, 213–229. https://doi.org/10.1016/S0022-1694(98)00254-6.

Beyene, M.T., Leibowitz, S.G., Pennino, M.J., 2021. Parsing weather variability and wildfire effects on the post-fire changes in daily stream flows: a quantile-based statistical approach and its application. Water Res. 57 https://doi.org/10.1029/2020WR028029.

Bladon, K.D., Emelko, M.B., Silins, U., Stone, M., 2014. Wildfire and the future of water supply. Environ. Sci. Technol. 48, 8936–8943. https://doi.org/10.1021/es500130g.

Blöschl, G., Ardoin-Bardin, S., Bonell, M., Dorninger, M., Goodrich, D., Gutknecht, D., Matamoros, D., Merz, B., Shand, P., Szolgay, J., 2007. At what scales do climate variability and land cover change impact on flooding and low flows? Hydrol. Process. 21, 1241–1247. https://doi.org/10.1002/hyp.6669.

Blount, K., Ruybal, C.J., Franz, K.J., Hogue, T.S., 2020. Increased water yield and altered water partitioning follow wildfire in a forested catchment in the western United States. Ecohydrology 13. https://doi.org/10.1002/eco.2170.

Bond, N., 2021. Package "hydrostats.".

Box, G., Jenkins, G., 1976. Time series analysis: Forecasting and control. Holden-Day series in time series analysis. Holden-Day.

Brunkal, H., Santi, P., 2017. Consideration of the Validity of Debris-Flow Bulking Factors. Geol. Soc. Am. 291–298 https://doi.org/10.2113/gseegeosci.23.4.291.

Budyko, M.I., 1974. Climate and Life. Academic Press.

Burke, M.P., Hogue, T.S., Kinoshita, A.M., Barco, J., Wessel, C., Stein, E.D., 2013. Pre- and post-fire pollutant loads in an urban fringe watershed in Southern California. Environ. Monit. Assess. 185, 10131–10145. https://doi.org/10.1007/s10661-013-3318-9.

Chang, M., 2012. Forest Hydrology: An Introduction to Water and Forests, Third Edition, 3rd ed. CRC Press, Boca Raton, FL.

Choudbury, B.J., 1999. Evaluation of an empirical equation for annual evaporation using field observations and results from a biophyscial model. J. Hydrol. 216, 99–110.

Chow, A.-T.-S., Karanfil, T., Dahlgren, R.A., 2021. Wildfires are Threatening Municipal Water Supplies. Eos Science News by AGU.

Collar, N.M., Saxe, S., Rust, A.J., Hogue, T.S., 2021. A CONUS-scale study of wildfire and evapotranspiration: Spatial and temporal response and controlling factors. J. Hydrol. 603, 25. https://doi.org/10.1016/j.jhydrol.2021.127162.

Cong, Z., Yang, D., Gao, B., Yang, H., Hu, H., 2009. Hydrological trend analysis in the Yellow River basin using a distributed hydrological model. Water Resour. Res. 45 https://doi.org/10.1029/2008WR006852.

Conner, M.M., Saunders, W.C., Bouwes, N., Jordan, C., 2016. Evaluating impacts using a BACI design, ratios, and a Bayesian approach with a focus on restoration. Environ. Monit. Assess. 188 https://doi.org/10.1007/s10661-016-5526-6.

Crawford, J.N., Mensing, S.A., Lake, F.K., Zimmerman, S.R., 2015. Late Holocene fire and vegetation reconstruction from the western Klamath Mountains, California, USA: a multi-disciplinary approach for examining potential human land-use impacts. Holocene 25, 1341–1357. https://doi.org/10.1177/0959683615584205.

David, A.T., Asarian, J.E., Lake, F.K., 2018. Wildfire smoke cools summer river and stream water temperatures. Water Resour. Res. 54, 7273–7290. https://doi.org/10.1029/2018WR022964.

de Haas, T., Ventra, D., Carbonneau, P.E., Kleinhans, M.G., 2014. Debris-flow dominance of alluvial fans masked by runoff reworking and weathering. Geomorphology 217, 165–181. https://doi.org/10.1016/j.geomorph.2014.04.028.

DeBano, L.F., Neary, D.G., Ffolliott, P.F., 1998. Fire Effects on Ecosystems. John Wiley & Sons.

Dias Lopes, J., Neiva Rodrigues, L., Acioli Imbuzeiro, H.M., Falco Pruski, F., 2019. Performance of SSEBop model for estimating wheat actual evapotranspiration in the Brazilian Savannah region. Int. J. Remote Sens. 40, 6930–6947. https://doi.org/10.1080/01431161.2019.1597304.

Dierauer, J., Whitfield, P., 2019. Package "FlowScreen.".

Downes, B.J., Barmuta, L.A., Fairweather, P.G., Faith, D.P., Keough, M.J., Lake, P.S., Mapstone, B.D., Quinn, G.P., 2002. Monitoring Ecological Impacts: Concepts and Practice in Flowing Waters. Cambridge University Press, Cambridge.

Ebel, B.A., Moody, J.A., Martin, D.A., 2012. Hydrologic conditions controlling runoff generation immediately after wildfire. Water Resour. Res. 48 https://doi.org/10.1029/2011WR011470.

Eberhardt, L.L., 1976. Quantitative ecology and impact assessment. Journal of Environmental Management 4, 27–70. https://doi.org/ERA-01-025919; EDB-76-074450.

Eidenshink, J., Schwind, B., Brewer, K., Zhu, Z.-L., Quayle, B., Howard, S., 2007. A project for monitoring trends in burn severity. Fire Ecol. 3, 3–21. https://doi.org/10.4996/fireecology.0301003.

Emelko, M.B., Stone, M., Silins, U., Allin, D., Collins, A.L., Williams, C.H.S., Martens, A. M., Bladon, K.D., 2016. Sediment-phosphorus dynamics can shift aquatic ecology and cause downstream legacy effects after wildfire in large river systems. Glob. Change Biol. 22, 1168–1184. https://doi.org/10.1111/gcb.13073.

Eskridge, R.E., Ku, J.Y., Rao, S.T., Porter, P.S., Zurbenko, I.G., 1997. Separating different scales of motion in time series of meteorological variables. Bull. Amer. Meteor. Soc. 78, 1473–1483. https://doi.org/10.1175/1520-0477(1997)078<1473:SDSOMI>2.0.CO;2.

Falcone, J., 2011. Geospatial attributes of gages for evaluating streamflow.

Ffolliott, P.F., Brooks, K.N., Neary, D.G., Tapia, R.P., Garcia-Chevesich, P., 2013. Soil erosion and sediment production on watershed landscapes: Processes and control. In: International Hydrological Programme of the Regional office for Science for Latin America and the Caribbean of the United Nations Educational, Scientific and Cultural Organizations (UNESCO), p. 73.

Florsheim, J.L., Chin, A., O'Hirok, L.S., Storesund, R., 2016. Short-term post-wildfire dry-ravel processes in a chaparral fluvial system. Geomorphology 252, 32–39. https://doi.org/10.1016/j.geomorph.2015.03.035.

U.S. Geological Survey, 2021. National Water Information System (NWIS): Web interface.

Gimbel, K.F., Puhlmann, H., Weiler, M., 2016. Does drought alter hydrological functions in forest soils? Hydrol. Earth Syst. Sci. 20, 1301–1317. https://doi.org/10.5194/hess-20-1301-2016.

Gleason, K.E., Nolin, A.W., 2016. Charred forests accelerate snow albedo decay: parameterizing the post-fire radiative forcing on snow for three years following fire. Hydrol. Process. 30, 3855–3870. https://doi.org/10.1002/hyp.10897.

Gleason, K.E., Nolin, A.W., Roth, T.R., 2013. Charred forests increase snowmelt: Effects of burned woody debris and incoming solar radiation on snow ablation. Geophys. Res. Lett. 40, 4654–4661. https://doi.org/10.1002/grl.50896.

Goeking, S.A., Tarboton, D.G., 2020. Forests and water yield: A synthesis of disturbance effects on streamflow and snowpack in western coniferous forests. J. Forest. 118, 172–192. https://doi.org/10.1093/jofore/fvz069.

Goulden, M.L., Bales, R.C., 2014. Mountain runoff vulnerability to increased evapotranspiration with vegetation expansion. PNAS 111, 14071–14075. https://doi.org/10.1073/pnas.1319316111.

Hallema, D.W., Sun, G., Bladon, K.D., Norman, S.P., Caldwell, P.V., Liu, Y., McNulty, S. G., 2017. Regional patterns of postwildfire streamflow response in the Western United States: The importance of scale-specific connectivity. Hydrol. Process. 31, 2582–2598. https://doi.org/10.1002/hyp.11208.

Hallema, D.W., Sun, G., Caldwell, P.V., Norman, S.P., Cohen, E.C., Liu, Y., Bladon, K.D., McNulty, S.G., 2018. Burned forests impact water supplies. Nat. Commun. 9, 1307. https://doi.org/10.1038/s41467-018-03735-6.

Hyndman, R.J., Athanasopoulos, G., 2018. Forecasting: principles and practice, Second, Edition. ed. OTexts, Melbourne, Australia.

Hyndman, R., 2022. Package "forecast.".

Jaramillo, F., Destouni, G., 2014. Developing water change spectra and distinguishing change drivers worldwide. Geophys. Res. Lett. 41, 8377–8386. https://doi.org/10.1002/2014GL061848.

Jin, Y., Randerson, J.T., Goetz, S.J., Beck, P.S.A., Loranty, M.M., Goulden, M.L., 2012. The influence of burn severity on postfire vegetation recovery and albedo change during early succession in North American boreal forests. J. Geophys. Res. 117 https://doi.org/10.1029/2011JG001886.

Keller, E., Adamaitis, C., Alessio, P., Anderson, S., Goto, E., Gray, S., Gurrola, L., Morell, K., 2019. Applications in geomorphology. Geomorphology 106729. https://doi.org/10.1016/j.geomorph.2019.04.001.

Keyantash, J.& N.C. for A.R.S., 2018. The Climate Data Guide: Standardized Precipitation Index (SPI). https://doi.org/Retrieved from https://climatedataguide.ucar.edu/climate-data/standardized-precipitation-index-spi.

Kinoshita, A.M., Hogue, T.S., 2015. Increased dry season water yield in burned watersheds in Southern California. Environ. Res. Lett. 10, 014003 https://doi.org/10.1088/1748-9326/10/1/014003.

Kirchner, J.W., Allen, S.T., 2020. Seasonal partitioning of precipitation between streamflow and evapotranspiration, inferred from end-member splitting analysis. Hydrol. Earth Syst. Sci. 24, 17–39. https://doi.org/10.5194/hess-24-17-2020.

Kirchner, J.W., Berghuijs, W.R., Allen, S.T., Hrachowitz, M., Hut, R., Rizzo, D.M., 2020. Streamflow response to forest management. Nature 578. https://doi.org/10.1038/s41586-020-1940-6. E12 E15.

Kurzweil, J.R., Metlen, K., Abdi, R., Strahan, R., Hogue, T.S., 2021. Surface water runoff response to forest management: Low-intensity forest restoration does not increase surface water yields. For. Ecol. Manage. 496, 119387 https://doi.org/10.1016/j.foreco.2021.119387.

Ladson, A.R., Brown, R., Neal, B., Nathan, R., 2013. A standard approach to baseflow separation using the Lyne and Hollick filter. Aust. J. Water Resour. 17, 25–34.
Lake, F.K., Wright, V., Morgan, P., McFadzen, M., McWethy, D., Stevens-Rumann, C., 2017. Returning fire to the land: Celebrating traditional knowledge and fire. J. Forest. 115, 343–353. https://doi.org/10.5849/jof.2016-043R2.
Lettenmaier, D.P., Alsdorf, D., Dozier, J., Huffman, G.J., Pan, M., Wood, E.F., 2015. Inroads of remote sensing into hydrologic science during the WRR era. Water Resour. Res. 51, 7309–7342. https://doi.org/10.1002/2015WR017616.
Lundquist, J.D., Dettinger, M.D., Cayan, D.R., 2005. Snow-fed streamflow timing at different basin scales: Case study of the Tuolumne River above Hetch Hetchy, Yosemite, California. Water Resour. Res. 41 https://doi.org/10.1029/2004WR003933.
Ma, Q., Bales, R.C., Rungee, J., Conklin, M.H., Collins, B.M., Goulden, M.L., 2020. Wildfire controls on evapotranspiration in California's Sierra Nevada. J. Hydrol. 590, 125364 https://doi.org/10.1016/j.jhydrol.2020.125364.
Maidment, D.R., 1993. Handbook of Hydrology. McGraw-Hill.
Mallakpour, I., Villarini, G., 2016. A simulation study to examine the sensitivity of the Pettitt test to detect abrupt changes in mean. Hydrol. Sci. J. 61, 245–254. https://doi.org/10.1080/02626667.2015.1008482.
Martin, D.A., 2016. At the nexus of fire, water and society. Phil. Trans. R. Soc. B 371, 20150172. https://doi.org/10.1098/rstb.2015.0172.
Martin, D., Tomida, M., Meacham, B., 2016. Environmental impact of fire. Fire Sci. Rev. 5, 5. https://doi.org/10.1186/s40038-016-0014-1.
McLeod, A.I., 2011. Package "Kendall.".
Milly, P.C.D., Betancourt, J., Falkenmark, M., Hirsch, R.M., Kundzewicz, Z.W., Lettenmaier, D.P., Stouffer, R.J., 2008. Stationarity is dead: whither water management? Science 319, 573–574.
Moody, J.A., Ebel, B.A., 2014. Infiltration and runoff generation processes in fire-affected soils. Hydrol. Process. 28, 3432–3453. https://doi.org/10.1002/hyp.9857.
Moody, J.A., Martin, D.A., 2009. Synthesis of sediment yields after wildland fire in different rainfall regimes in the western United States. Int. J. Wildland Fire 18, 96–115. https://doi.org/10.1071/WF07162.
Mueller, E.R., Smith, E.M., Pitlick, J., 2010. Lithology-controlled evolution of stream bed sediment and basin-scale sediment yields in adjacent mountain watersheds, Idaho, USA. Earth Surface Processes and Landforms 41, 1869–1883. https://doi.org/DOI: 10.1002/esp.3955.
Murphy, B.P., Yocom, L.L., Belmont, P., 2018. Beyond the 1984 perspective: narrow focus on modern wildfire trends underestimates future risks to water security. Earth's Future 6, 1492–1497. https://doi.org/10.1029/2018EF001006.
Neary, D.G., Ryan, K.C., DeBano, L.F., 2005. Wildland fire in ecosystems: effects of fire on soils and water (No. RMRS-GTR-42-V4). U.S. Department of Agriculture, Forest Service, Rocky Mountain Research Station, Ft. Collins, CO. https://doi.org/10.2737/RMRS-GTR-42-V4.
Nolan, R.H., Lane, P.N.J., Benyon, R.G., Bradstock, R.A., Mitchell, P.J., 2014. Changes in evapotranspiration following wildfire in resprouting eucalypt forests. Ecohydrology. https://doi.org/10.1002/eco.1463.
Nunes, J.P., Doerr, S.H., Sheridan, G., Neris, J., Santín, C., Emelko, M.B., Silins, U., Robichaud, P.R., Elliot, W.J., Keizer, J., 2018. Assessing water contamination risk from vegetation fires: Challenges, opportunities and a framework for progress. Hydrol. Process. 32, 687–694. https://doi.org/10.1002/hyp.11434.
Nyman, P., Box, W.A.C., Stout, J.C., Sheridan, G.J., Keesstra, S.D., Lane, P.N.J., Langhans, C., 2020. Debris-flow-dominated sediment transport through a channel network after wildfire. Earth Surf. Process. Landforms 45, 1155–1167. https://doi.org/10.1002/esp.4785.
Omernik, J.M., Griffith, G.E., 2014. Ecoregions of the conterminous United States: Evolution of a hierarchical spatial framework. Environ. Manage. 54, 1249–1266. https://doi.org/10.1007/s00267-014-0364-1.
Oregon State University, 2019. Descriptions of PRISM Spatial Climate Datasets for the Conterminous United States [WWW Document]. URL https://prism.oregonstate.edu/documents/PRISM_datasets.pdf (accessed 10.14.20).
Overpeck, J.T., Udall, B., 2020. Climate change and the aridification of North America. PNAS 117, 11856–11858. https://doi.org/10.1073/pnas.2006323117.
Parks, S.A., Abatzoglou, J.T., 2020. Warmer and drier fire seasons contribute to increases in area burned at high severity in western US forests from 1985 to 2017. Geophys. Res. Lett. 47 https://doi.org/10.1029/2020GL089858.
Pohlert, T., 2020. Package "Trend.".
Pomeroy, J., Fang, X., Ellis, C., 2012. Sensitivity of snowmelt hydrology in Marmot Creek, Alberta, to forest cover disturbance. Hydrol. Process. 26, 1891–1904. https://doi.org/10.1002/hyp.9248.
Poon, P.K., Kinoshita, A.M., 2018. Spatial and temporal evapotranspiration trends after wildfire in semi-arid landscapes. J. Hydrol. 559, 71–83. https://doi.org/10.1016/j.jhydrol.2018.02.023.
Pugh, E., Gordon, E., 2013. A conceptual model of water yield effects from beetle-induced tree death in snow-dominated lodgepole pine forests. Hydrol. Process. 27, 2048–2060. https://doi.org/10.1002/hyp.9312.
Roderick, M.L., Farquhar, G.D., 2011. A simple framework for relating variations in runoff to variations in climatic conditions and catchment properties: RUNOFF SENSITIVITY AND CLIMATE CHANGE. Water Resour. Res. 47 https://doi.org/10.1029/2010WR009826.
Running, S., Mu, Q., Zhao, M., 2017. MOD16A2 MODIS/Terra Net Evapotranspiration 8-Day L4 Global 500m SIN Grid V006 [Data set]. NASA EOSDIS Land Processes DAAC. https://doi.org/10.5067/MODIS/MOD16A2.006.
Rust, A., Hogue, T., Saxe, S., Mccray, J., 2018. Post-fire water-quality response in the western United States. Int. J. Wildland Fire 27. https://doi.org/10.1071/WF17115.
Ryu, Y., Baldocchi, D.D., Ma, S.Y., Hehn, T., 2008. Interannual variability of evapotranspiration and energy exchange over an annual grassland in California. J. Geophys. Res. Atmos. 113. https://doi.org/10.1029/2007JD009263.
Santi, P.M., Morandi, L., 2013. Comparison of debris-flow volumes from burned and unburned areas. Landslides 10, 757–769. https://doi.org/10.1007/s10346-012-0354-4.
Saxe, S., Hogue, T.S., Hay, L., 2018. Characterization and evaluation of controls on post-fire streamflow response across western US watersheds. Hydrol. Earth Syst. Sci. 22, 1221–1237. https://doi.org/10.5194/hess-22-1221-2018.
Senay, G.B., 2018. Satellite psychrometric formulation of the Operational Simplified Surface Energy Balance (SSEBop) model for quantifying and mapping evapotranspiration. Appl. Eng. Agric. 34. https://doi.org/10.13031/aea.12614.
Senay, G.B., Bohms, S., Singh, R.K., Gowda, P.H., Velpuri, N.M., Alemu, H., Verdin, J.P., 2013. Operational evapotranspiration mapping using remote sensing and weather datasets: a new parameterization for the SSEB approach. JAWRA J. Am. Water Resour. Assoc. 49, 577–591. https://doi.org/10.1111/jawr.12057.
Senay, G.B., Friedrichs, M., Singh, R.K., Velpuri, N.M., 2016. Evaluating Landsat 8 evapotranspiration for water use mapping in the Colorado River Basin. Remote Sens. Environ. 185, 171–185. https://doi.org/10.1016/j.rse.2015.12.043.
Sexstone, G.A., Clow, D.W., Fassnacht, S.R., Liston, G.E., Hiemstra, C.A., Knowles, J.F., Penn, C.A., 2018. Snow sublimation in mountain environments and its sensitivity to forest disturbance and climate warming. Water Resour. Res. 54, 1191–1211. https://doi.org/10.1002/2017WR021172.
Shakesby, R., Doerr, S., 2006. Wildfire as a hydrological and geomorphological agent. Earth Sci. Rev. 74, 269–307. https://doi.org/10.1016/j.earscirev.2005.10.006.
Sharma, D.N., Tare, V., 2018. Evapotranspiration estimation using SSEBop method with Sentinel-2 and Landsat-8 dataset. Int. Arch. Photogramm. Remote Sens. Spatial Inf. Sci. XLII–5, 563–566. https://doi.org/10.5194/isprs-archives-XLII-5-563-2018.
Shumway, R.H., Stoffer, D.S., 2016. Time series analysis and its applications, Fourth Edition. ed. Springer.
Singh, R., Senay, G.B., 2015. Comparison of four different energy balance models for estimating evapotranspiration in the midwestern United States. Water 8, 9. https://doi.org/10.3390/w8010009.
Skiles, S.M., Painter, T.H., 2015. A 9-yr record of dust on snow in the Colorado river basin. In: 12th Biennial Conf. of Science and Management on the Colorado Plateau 1. https://doi.org/10.3133/sir20155180.
Slinski, K.M., Hogue, T.S., Porter, A.T., McCray, J.E., 2016. Recent bark beetle outbreaks have little impact on streamflow in the Western United States. Environ. Res. Lett. 11, 074010 https://doi.org/10.1088/1748-9326/11/7/074010.
Soil Survey Staff, NRCS, USDA, 2021. Web Soil Survey. Available online at the following link: http://websoilsurvey.sc.egov.usda.gov/. https://doi.org/Accessed April 2021.
STHDA, 2018. Linear regression assumptions and diagnostics in R: Essentials [WWW Document]. URL http://www.sthda.com/english/articles/39-regression-model-diagnostics/161-linear-regression-assumptions-and-diagnostics-in-r-essentials/.
Sun, L., Baker, J.C.A., Gloor, E., Spracklen, D., Boesch, H., Somkuti, P., Maeda, E., Buermann, W., 2019. Seasonal and inter-annual variation of evapotranspiration in amazonia based on precipitation, river discharge and gravity anomaly data. Front. Earth Sci. 7, 32. https://doi.org/10.3389/feart.2019.00032.
Tague, C.L., Moritz, M., Hanan, E., 2019. The changing water cycle: The eco-hydrologic impacts of forest density reduction in Mediterranean (seasonally dry) regions. WIREs Water 6. https://doi.org/10.1002/wat2.1350.
Thornton, M.M., Thornton, P.E., Wei, Y., Mayer, B.W., Cook, R.B., Vose, R.S., 2018. Daymet: Monthly climate summaries on a 1-km grid for North America, Version 3. ORNL DAAC, Oak Ridge, Tennessee, USA. https://doi.org/10.3334/ornldaac/1345.
Trapletti, A., Hornik, K., LeBaron, B., 2021. Package 'tseries.'.
USDA Forest Service, USDI, 2021. Landfire: Landscape fire and resource management planning tools [WWW Document]. URL https://www.landfire.gov/about.php (accessed 8.17.20).
van der Wiel, K., Bintanja, R., 2021. Contribution of climatic changes in mean and variability to monthly temperature and precipitation extremes. Commun. Earth Environ. 2, 1. https://doi.org/10.1038/s43247-020-00077-4.
Vourlitis, G.L., de Souza Nogueira, J., de Almeida Lobo, F., Sendall, K.M., de Paulo, S.R., Antunes Dias, C.A., Pinto, O.B., de Andrade, N.L.R., 2008. Energy balance and canopy conductance of a tropical semi-deciduous forest of the southern Amazon Basin: TROPICAL FOREST ENERGY BALANCE. Water Resour. Res. 44 https://doi.org/10.1029/2006WR005526.
Wickham, J., Homer, C., Vogelmann, J., McKerrow, A., Mueller, R., Herold, N., Coulston, J., 2014. The Multi-Resolution Land Characteristics (MRLC) consortium — 20 years of development and integration of USA National Land Cover Data. Remote Sensing 6, 7424–7441. https://doi.org/10.3390/rs6087424.
Williams, A.P., Livneh, B., McKinnon, K.A., Hansen, W.D., Mankin, J.S., Cook, B.I., Smerdon, J.E., Varuolo-Clarke, A.M., Bjarke, N.R., Juang, C.S., Lettenmaier, D.P., 2022. Growing impact of wildfire on western US water supply. PNAS 119, 8. https://doi.org/10.1073/pnas.2114069119.
Wine, M.L., Cadol, D., 2016. Hydrologic effects of large southwestern USA wildfires significantly increase regional water supply: fact or fiction? Environ. Res. Lett. 11.
Wine, M.L., Makhnin, O., Cadol, D., 2018. Nonlinear long-term large watershed hydrologic response to wildfire and climatic dynamics locally increases water yield. Earth's Future 6, 997–1006. https://doi.org/10.1029/2018EF000930.
Xu, X., Yang, D., Yang, H., Lei, H., 2014. Attribution analysis based on the Budyko hypothesis for detecting the dominant cause of runoff decline in Haihe basin. J. Hydrol. 510, 530–540. https://doi.org/10.1016/j.jhydrol.2013.12.052.

Zeileis, A., 2019. Package "dynlm:" Dynamic Linear Regression.
Zhou, C., van Nooijen, R., Kolechkina, A., Hrachowitz, M., 2019. Comparative analysis of nonparametric change-point detectors commonly used in hydrology. Hydrol. Sci. J. 64, 1690–1710. https://doi.org/10.1080/02626667.2019.1669792.
Zhuang, Y., Fu, R., Santer, B.D., Dickinson, R.E., Hall, A., 2021. Quantifying contributions of natural variability and anthropogenic forcings on increased fire weather risk over the western United States. PNAS 118. https://doi.org/10.1073/pnas.2111875118 e2111875118.